REPUBLIC OF AZERBAIJAN

On the rights of the manuscript

ABSTRACT

of the dissertation for the degree of Doctor of Science

PHYSICO-CHEMICAL BASIS OF THE SYNTHESIS OF LAYERED DOUBLE HYDROXIDES, TRANSITION METAL OXIDES AND SULFIDES POLYMER NANOCOMPOSITES

Speciality: 2317.01- Nanochemistry and nanomaterials

Field of science: Chemistry

Applicant: **Ofeliya Oqtay Balayeva**

Baku – 2024

The work was performed at Chemistry of high molecular compounds department of Baku State University.

Scientific consultant: doctor of chemical sciences, professor
Abdulsaid Abdulhamid Azizov

Official opponents: Active member of ANAS,
Doctor of chemical sciences, professor
Vagif Maharram Abbasov;

Corresponding member of ANAS,
Doctor of chemical sciences, professor
Islam Israfil Mustafayev;

Corresponding member of ANAS,
Doctor of chemical sciences, professor
Mahammad Baba Babanlı;

Corresponding member of ANAS,
Doctor of chemical sciences, assoc. professor
Aliaddin Dayyan Abbasov.

Dissertation council BED 2.16 of Supreme Attestation Commission under the President of the Republic of Azerbaijan operating at Baku State University

Chairman of the
Dissertation council: Doctor of Chem. Sci., prof.
Ibrahim Garib Mammadov

Scientific secretary of the
Dissertation council: Doctor of Chem. Sci., assoc. prof.
Farid Nadir Naghiyev

Chairman of the
Scientific seminar: Active member of ANAS,
Doctor of Chem. Sci., prof.
Vagif Majid Farzaliyev

Azərbaycan Respublikasının Elm və Təhsil Nazirliyi
BAKI DÖVLƏT UNİVERSİTETİ p.h.ş.
Ministry of Science and Education of the Republic of Azerbaijan
Baku State University l.e.p.l.
ELMİ KATİB
SCIENTIFIC SECRETARY
İmzanı təsdiq edirəm:
(S.A.A.)
„16" 05 2024

GENERAL CHARACTERISTICS OF THE WORK

Relevance of the topic and degree of development. Recent studies show that the interest in polymer-based nanocomposite materials is increasing day by day due to the intensive development of nanotechnology. The integration of devices with special properties into intelligent and self-managing systems is one of the main goals for the possible future of electronics, optics and photonics.The majority of objects in nanoscience are metal hydroxides, oxides, sulfides, and polymer nanocomposites.

Layered double hydroxides (LDHs) have been promising materials are used as an ion exchanger, adsorbent and catalyst in catalysis, pharmaceuticals, biochemistry, photonics, electrochemical processes, sorption and photo-, electro-, sono-degradation of organic and inorganic pollutants from aqueous solutions. Recently, the preparation of polymer/LDH nanocomposites is very interesting. Depending on the polymer and the method it is possible to expand the distance between the hydroxide layers by inserting polymer macromolecules into the interlayer space of LDHs [1,2.]

Transition metal oxide semiconductor nanostructures have antimicrobial activity, sensing ability, adsorption propertie, and catalytic performance which attracted great interest as a promising nanomaterials. Due to the effective change of their properties depending on their size and shape and their photovoltaic, catalytic, photoelectric, photosensor, etc. performance, synthesis and modification of ternary metal sulfide semiconductor nanoparticles has attracted many scientists in recent years. Currently, there is still a need to investigate more selective and effective photocatalysts for multipollutants containing organic and inorganic contaminants.

---

[1] Béres, A. Layered double hydroxides and their pillared derivatives – Materials for solid base catalysis; synthesis and characterization / A. Béres, I. Pálinkó, I. Kiricsi [et al.] // Applied Catalysis A: General, - 1999. 182, - p. 237–247.

[2] Bukhtiyarova, M.V. A review on effect of synthesis conditions on the formation of layered double hydroxides / M. V. Bukhtiyarova // Journal of Solid State Chemistry, - 2019. 269, - p. 494–506. https://doi.org/10.1016/j.jssc.2018.10.018

The object and subject of the research. Polyvinyl alcohol (PVA), nitrile butadiene rubber (NBR) and functionalized nitrile rubber (FNBR) were used as polymer matrix, CoCr-LDH, CoAl-LDH, ZnAl-LDH, NiAl-LDH, NiZnAl-LDHs, CdZnAl-LDH, ZnO, $Zn_6Al_2O_9$, ZnS, CdS, Cu_xS,$Ni_xZn_{1-x}S$, $Cd_xZn_{1-x}S$, $CuCdS_2$ as hydroxide, oxide and sulfide nanoparticles, active- (Ca, Sr), transition- (Co, Cu, Cd, Ni, Pb, Fe), noble- (Ag) and rare earth- (La) elements were selected as additive elements (dopants). The main subject of the dissertation work is the preparation of new nanocomposites based on the listed nanoparticles and polymers, their physico-chemical investigation, study the size-structure-property relationships, sorption, photocatalytic oxidation and other areas of application.

Aims and objectives of the research: Studing the effect of reaction parameters and the ratio of metal ions on the synthesis of ZnAl, CoAl, CoCr, NiZnAl, CdZnAl-based LDHs and oxides by using alkaline solutions different concentrations; preparing their nanocomposites with differend polymers; investigating their sorption and photocatalytic activity; doping the obtained LDHs with various elements and investigating the effect of the nature of dopant metals on the photoactivity; studing the sorption and photodegradation of synthetic hazardous dyes, phenol and toxic derivatives of phenol from aqueous solutions by the obtained nanocomposites; synthesize their ternary sulfides and heterostructures and explore their application in photocatalysis knowing their sensitivity to light and applications in many fields such as photoelectrics, sensors and thermal agents.

Research methods. SILAR, co-precipitation, co-formation, hydrolysis with urea, ion exchange, intercalation, thermal deposition, ultrasonic-, magnetic- and mechanical-mixing, oxidation-chlorophosphorylation and doping were applied as synthesis and modification methods. Modern and traditional research methods like scanning electron microscope (SEM), X-ray diffractometer (XRD), ultraviolet (UV) spectroscopy, infrared (IR) spectroscopy, electron paramagnetic resonance (EPR) spectroscopy, Brunauer-Emmet-Teller (BET), thermogravimetric analysis (TGA), differential scanning calorimeter (DSC)), photoluminescence (PL) and optical emission spectroscopy (ICP-OES) have been applied for the investigation of the obtained nanocomposites.

The main provisions for the defense:

1. It has been shown that it is possible to influence the properties, size, band gap, morphology, sorption and photocatalytic activity of nanoparticles by changing the reaction parameters, the sequence of processing of reagents, the concentration ratio of metal ions, intercalating agents, the nature of anions and the percentage of the polymer.

2. In a very highly concentrated alkaline solution, the reaction resulted in high crystallization even when the ionic radii of the metals forming CoCr-LDH nanocomposites are close to each other.

3. The characteristic peaks of the ZnO phase along with the hydrotalcite structure are related to the amphoteric properties of Al according to the XRD analysis of ZnAl-LDH$_{5M}$ and ZnAl-LDH$_{2M}$ nanocomposites synthesized using high concentrations of alkaline solution (2M and 5M NaOH).

4. The diffraction peak corresponding to PVS (19.17°) shifted to a higher diffraction angle (20°) with the formation of ZnAl-LDH/PVA nanocomposite by co-formation method and a crosslinking of PVA through LDH has been happened. Two types of optical electronic transition related to the Zn-O bond for ZnO and $Zn_6Al_2O_9$ nanocrystals in the nanocomposite between the filled 2p orbitals of oxygen and the 4p and 4s orbitals of Zn, as well as the electronic transition between the filled 2p orbitals of oxygen and the empty 3s and 3p orbitals of the aluminum ion in the $Zn_6Al_2O_9$ crystal is defined.

5. The maximum sorption capacity of ZnAl mixed oxide/PVA for Pb^{2+} ions was 1000 mg/g in 180 minutes, and the adsorption degree reached to ~97%.

6. The shift of the diffraction peaks belonging to LDH to lower angles and the increase in the average size of its particles after the sorption of Tartrazine, Ponso 4R (P4R) and Patent blue V (PB-V) dyes in ZnAl-LDH/PVS nanocomposite are explained by the intercalation of LDH layers. The efficiency of photodegradation

reached the maximum value (89.7%) at the initial concentration of P4R dye at 12 mg/l, the value of the Langmuir constant (K_L = 0.102) was close to the value of the Langmuir-Hinshelwood constant ($K_{L\text{-}H}$ = 0.094). Since the active centers on a homogeneous surface have the same adsorption energy, the adsorption of zwitterion molecules on LDHs increased due to electrostatic forces.

7. The wide band gap width (~3.6 eV) observed for the first time for CuCdS2 nanostructures was explained by the formation of smaller particles in the FNBR matrix with limited volume.

8. During the alternating synthesis of $Cd_xZn_{1-x}S$ nanoparticles by the SILAR method, heterostructures were formed. The formation of new peaks corresponding to Cd^{2+} and Cd^0 by carrying out the nucleation with CdS is due to the fact that cadmium is less active than zinc and tends to reduction.

9. The average size of nanocrystallites increased from 8 nm to ~20 nm and the dislocation density (δ) decreased from 0.0127 nm^2 to ~0.003 nm^2 with non-covalent doping of C_{60} to ZnAl-LDH/PVA nanocomposite. Photodegradation of Methylene blue and Congo red on the C_{60}/ZnAl-LDH/PVA accompanied by $\bullet O_2^{-}$ and •OH, respectively.

10. The doping of ZnAl LDH/PVA nanocomposites with different metal ions was carried out by impregnation method. It was determined that the nature of doping elements has a direct effect on the recombination of h+ and e- pairs.

Scientific novelty of the research. For the first time:

1. Although the radii of the metal ions forming CoCr-LDH are close to each other, the reaction in highly concentrated alkaline solutions (10M and 20M NaOH) resulted in high crystallization and the formation of LDH;

2. ZnAl-LDH and ZnAl-oxide nanostructures can be promising materials in optical devices, gas sensors, photosensors, and photocatalytic applications, as they have a significantly lower band gap than their counterparts.

3. The thermal annealing of $CuCdS_2$ nanoparticles was processed, and the formation of a new oxide phase ($CuCdO_2$) was observed.

4. Compared with other adsorbents, ZnO-Al_2O_3/PVA nanocomposite showed high adsorption-desorption capacity to effectively remove lead (II) ions (Pb^{2+}) from wastewater ($q_{max.}$ = 1000mg/g).

5. The sorption and photodegradation efficiency of synthetic food dyes like Tartrazine, P4R and PB-V with ZnAl-LDH/PVA nanocomposite was very high. The photocatalytic efficiency of the ZnAl-LDH/PVA nanocomposite increased intensively in each subsequent period, and the photodegradation degree of tartrazine reached 99.99% after 4th and subsequent period.

6. Doping with C_{60} and various elements (Ca, Sr, Co, Cu, Cd, Ni, Pb, Fe, Ag, La) and co-extraction with anionic dyes were applied in order to increase the adsorption and photodegradation of cationic dyes onto anionic clays like LDHs. The sorption and photodegradation degree increased significantly.

Theoretical and practical significance of the research:

1. The basal distance of sodium stearate intercalated CoCr-LDH increased from 7.366 Å to 25.214 Å. The expansion of the basal distance is favorable for obtaining new polymer nanocomposites with a high barrier effect. Industrial scale application of thermally resistant, flame retardant and gas impermeable ultrathin nanocomposites obtained in this way is very important.

2. Since ZnAl-LDH and ZnAl-oxide structures show a significantly lower band gap (E_g) compared to other analogs, the resulting nanomaterials are promising for low-energy photocatalytic devices, gas sensors, and photosensors.

3. The determination of transparency in thin films made of ZnAl-LDH/PVA nanocomposites obtained by ultrasonic mixing increases their application to thermotropic materials. For ZnAl-LDH_{urea} sample, the size of the nanoparticles is high (d = 22.37 nm), "a" lattice parameter is small (a = 2.96 Å) which is reduces the electronic transition energy (E_{g2} = 3.0 eV) and increase the potential application of the material in optical and electronic work. The obtained ZnAl-LDHs can be used as photocatalytic and electrocatalytic active materials in hydrogen fuel cells, power transmissions and photodegradation of organic pollutants.

4. $CuCdS_2$ nanoparticles with high band gap energy are used in power devices, radio and other energy conversions, light emitting diodes (LEDs), semiconductor lasers, etc.

5. CdS/FNBR, ZnS/FNBR, and $CdZnS_2$/FNBR nanocomposites can be applied in solar panels, photosensitive semiconductor devices, and gas sensors exhibiting high crystallization, optical properties, thermal and mechanical stability.

6. ZnAl mixed oxide/PVA nanocomposites are suitable, safe and cost-effective sorbents for the sorption of heavy metals from aqueous solutions and can be applied for environmental purposes.

7. The sorption capacity, photocatalytic activity and selectivity of the regenerated nanocomposite do not decrease with use.

8. Various doping elements and C_{60}-doped LDHs nanocomposites can be applied on an industrial scale in the sorption and photodegradation of cationic dye molecules.

Approbation and implementation: The results of the dissertation were published in 63 scientific works (24 articles and 39 abstracts) in local and foreign journals. 14 of the articles were published in journals indexed in Web of Science Clarivate Analytics and 2 in Scopus system and 315 citations were made to them.

The main results of the dissertation work were presented at republican and international conferences held in ***Azerbaijan, Turkey and Georgia***: Acad. International conference dedicated to the 110th anniversary of the birth of M. Nagiyev, ANAS, ***Baku*** 2018; II, III and V International scientific conference of young researchers. Baku Engineering University; ***Baku*** 2018, 2019, 2021; 12th, 13th, 15th International, I, II Republican Scientific Conference of young researchers dedicated to the 95th, 96th, 98th, 99th, 100th anniversary of the birth of national leader Heydar Aliyev, BSU, ***Baku*** 2018, 2019, 2021, 2022, 2023 ; The Chemistry of Coordination Compounds, Dedicated to the 85th anniversary of the Department of Analytical Chemistry, BSU, ***Baku*** 2020; Current Problems of Chemical Engineering dedicated to the 100th anniversary of the Azerbaijan State Oil and Industry University, ASOIU, ***Baku*** 2020; 2nd International Conference on Light and Light-based Technologies (ICLLT) Gazi University, ***Ankara***, 2021; Modern Trends in Physics.

Baku 2021; 6th International Conference "Nanotechnology". ***Tbilisi***, 2021; 1st International symposium on recent advances in fundamental and applied sciences (ISFAS-2021) Atatürk University, ***Erzurum***, 2021; 1st international congress on natural sciences (ICNAS-2021)" Atatürk University ***Erzurum***, 2021; I, II, IV, V ASES international health, engineering and sciences congress ***Ankara***, ***Eskisehir***, ***Kayseri*** 2022, 2023; International Conference: Modern Problems of Theoretical & Experimental Chemistry, ***Baku*** 2022; 9th International Conference on Materials Science and Nanotechnology for Next Generation Gazi University, ***Ankara*** 2022; Mediterranean International Conference on Research in Applied Sciences, ***Antalya***, 2022, IV Baskent International conference on multidisciplinary studies, ***Ankara*** 2023;

Name of the organization where the dissertation has been performed: The dissertation work was carried out at Baku State University,"Chemistry of high molecular compounds" department.

Personal contribution of the author. Setting issues, collecting, analyzing and reviewing literature data, planning research and conducting experiments, preparing samples, systematizing, analyzing and explaining results, conducting of physico-chemical analysis, preparing, writing and submitting articles and conference materials are carried out with the direct participation of the author.

Volume, structure and the main content of the dissertation: Dissertation consists of 398 pages (375,276 signs), introduction (30,548), 7 chapters, (first chapter - 99,803 signs, second chapter - 43,433 marks, third chapter - 30,706 signs, fourth chapter - 9,690 marks, fifth chapter -50 486 signs, the sixth chapter - 54 920 signs, the seventh chapter - 40314 signs) main results (15 376) and 481 references. 121 figures and 54 tables and diagrams also include to the the dissertation.

CONTENTS OF THE WORK

In the introduction, the relevance, main purpose, scientific novelty, theoretical and practical importance of the work, and the defended provisions are explained.

In the first chapter, extensive literature sources related to the topic of the study were investigated, systematized, classified analyzed and interpreted. Synthesis methods and modification, properties and application of LDHs, nanoparticles of binary and ternary transition metal sulfides and oxides and their polymer nanocomposites were considered, the effect of technological parameters on the properties of nanocomposites, size-property-structure relationships were investigated, directions for the relevance of the research were determined.

The main results obtained from the literature analysis are as follows: The production of nano-sized LDHs with high crystallization depends on the pH of the environment, the nature of the alkaline agents, the technological conditions, methods, ionic radius of the metal ions, intercalating anions, and the rate of co-precipitation. It was determined that, LDHs obtained by co-precipitation of metals with close ionic radii show high crystallization. Co-precipitation and high crystallization can be achieved by using a highly concentrated alkaline solution for LDHs containing divalent and trivalent metals with sharply different ionic radii.

Nanocomposites formed by LDHs with polymers are industrially important materials due to their mechanical, thermal, electrical, surface, structure, etc. properties. Depending on the polymer and the method, it is possible to extend the distance between the double hydroxide layers in which the LDHs are formed, from 0.2 nm to 5 nm by the intercalating of LDHs with polymer macromolecules. Significant degree of intercalation can be achieved by controlling the nature, structure and size of the intercalating agents, and the parameters of the medium.

Nanostructures of transition metals binary and ternary oxides are semiconducting materials and they have high photocatalytic activity, sensing ability, sorption, antimicrobial, etc. properties. They can be synthesized from LDHs and sulfides by direct oxidation. At this time, the obtained nanostructures partially retain the size and properties of the original material and it is possible to create a memory effect by their modification.

While the production of ternary sulfide nanoparticles consisting of elements similar in nature and properties can be achieved under mild conditions, the co-sulfidation of metals with sharp differences in nature requires special conditions and a highly controlled environment.

In the second chapter, the course of all the experimental work conducted during the research, calculation and determination of crystal lattice parameters of nanomaterials, band gap, sorption isotherms, kinetics of sorption and photodegradation, research methods, preparation of samples for analysis were given.

Synthesis of CoCr, CoAl, ZnCr, ZnAl, CdAl, NiAl and FeAl-based LDHs and preparation of polymer nanocomposites: Mixed solutions of 0.015 mol of divalent metal salts and 0.005 mol trivalent metal salts [$Al_2(SO_4)_3 \cdot 18H_2O$ (or $Cr_2(SO_4)_3 \cdot 9H_2O$)] were prepared and 0.1 mol of urea/ammonium citrate and 10% PVA was added to the obtained mixtures separately. The mixed solutions were titrated with 1 M $NaHCO_3$ and 2 M NaOH, 5M NaOH solution was added dropwise to bring pH 10 and heated at 90°C for 72 h. The samples were marked as $Me(II)Me(III)\text{-}LDH_{(urea.)}$, $Me(II)Me(III)LDH_{(ACTB)}$ *and* $Me(II)Me(III)\ LDH_{(urea)}$/PVA.

Modification of CoCr LDHs with stearic acid (SA) and sodium stearate (NaSt). First, SA solutions in alcohol and NaSt in water were prepared, and CoCr LHs were added and heated at 90°C for 4 days. Intercalation was accelerated by applying high mixing and agitation. The obtained nanocomposite samples were marked SA-CoCr-LDH (100°C), SA-CoCr-LDH(25°C), SA-CoCr-LDH(90°C) and NaSt-CoCr-LDH(100°C), NaSt-CoCr-LDH(90°C), NaSt-CoCr-LDH (25°C).

Synthesis of LDHs in highly concentrated alkaline medium. After preparing the above-mentioned mixed salt solutions, they were precipitated with 2, 5, 10 and 20 M NaOH solutions. According to the concentration of NaOH, the nanocomposite samples were marked as $Me(II)Me(III)\text{-}LDH_{(2M)}$, $Me(II)Me(III)\text{-}LDH_{(5M)}$, $Me(II)Me(III)\text{-}LDH_{(10M)}$, *and* $Me(II)Me(III)\text{-}LDH_{(20M)}$.

Synthesis of ZnO, $Zn_6Al_2O_9$ and ZnO- Al_2O_3 binary and ternary oxide nanocrystals and preparation of their nanocomposites with PVA. Zinc aluminum-based LDH (ZnAl-LDH), -oxide (ZnO), -mixed oxide ($Zn_6Al_2O_9$) and nanocomposites with PVA were synthesized by co-precipitation and co-formation methods. The samples were marked as ZnAl-LDH$_{2M}$, ZnAl-LDH$_{5M}$, ZnAl-LDH$_{urea(2)}$ and ZnO-Al$_2$O$_3$/PVA.

Exsitu preparation of ZnAl-LDH/PVA nanocomposites films. Powdered ZnAl-LDH$_{carb.}$ nanoparticles 0.5% (0.05g); 1% (0.1g) and 3% (0.3g) were weighed, 5ml of distilled water and 10ml of 10% solution of PVA were added to each of them, mixed mechanically for 24 hours and ultrasonically for 10 minutes. The nanocomposite samples were marked as 0.1% ZnAl-LDH$_{carb.}$+PVA, 1%ZnAl-LDH$_{carb.}$+PVA, 3%ZnAl-LDH$_{carb.}$+ PVA according to the amount of PVA in the content.

Crystallization of ZnAl-LDH in PVA solution. The mixture of salt solutions prepared according to the above procedure was added to 40 ml of 10% solution of PVA, mixed with a magnetic stirrer for 30 minutes and titrated with 25 ml of 5M NaOH solution. The obtained white mixture was heated at 90°C for 72 hours, washed with distilled water and dried in air, marked as ZnAl-LDH/PVA.

Doping of ZnAl-LDH/PVA nanocomposites with different metals. Doping of ZnAl-LDH/PVA with alkaline earth (Ca, Sr), transition (Co, Cu, Cd, Ni, Pb, Fe), noble (Ag) and rare earth (La) elements was carried out by the impregnation method. Well-dried ZnAl-LDH/PVA nanocomposites was added to 1 mM of $FeSO_4 \cdot 7H_2O$, $Ni(NO_3)_2 \cdot 6H_2O$, $Co(NO_3)_2 \cdot 6H_2O$, $Pb(NO_3)_2$, $Cd(NO_3)_2 \cdot 4H_2O$, $CuSO_4 \cdot 5H_2O$, $Ca(NO_3)_2$, $Sr(NO_3)_2$ x $6H_2O$ and $AgNO_3$ salt solutions and kept in the dark for 4 hours, heated at 90°C for 3 hours, cooled to room temperature, dried at room conditions and thermally annealed at 150°C for 7 hours. The physical and chemical properties, sorption and photocatalytic activity of the obtained nanocomposites were studied. The samples were designated as Me/ZnAl-LDH/PVA nanocomposites.

Fabrication of FNBR-based CdS, ZnS and CdZnS nanocomposites. Functionalized nitrile rubber (FNBR) is a polymer containing phosphonic (-PO(OH)2) and phosphate (-O-PO(OH)2) groups was obtained by oxidation-chlorophosphorization method of NBR. Functionalized nitrile rubber (FNBR) is a polymer containing phosphonic (-PO(OH)2) and phosphate (-O-PO(OH)2) groups was obtained by oxidation-chlorophosphorization method of NBR. To obtain binary and ternary sulfides, 1M 50 ml ZnSO4×7H2O and 1M 50 ml $CdCl_2$×2.5H2O solutions in water were first prepared, and 0.1 g of FNBR was added to it. After keeping the polymers into the salt solutions for 24 hours, they were washed with distilled water and 10 ml of 0.1 M Na2S · 9H2O solution was added to each one. The process was carried out in 5 and 15 SILAR periods. The obtained nanocomposites were named as CdS/FNBR, ZnS/FNBR, $Cd_{0.5}Zn_{0.5}S$/FNBR, $Cd_{0.75}Zn_{0.25}S$/FNBR, $Cd_{0.25}Zn_{0.75}S$/ FNBR, the scheme of the experiment is shown in **Figure** 1.

Preparation of $CuCdS_2$ ternary sulfide nanocomposite based on FNBR. $CuCl_2 \cdot 2H_2O$), $CdCl_2 \cdot 2.5H_2O$ and $Na_2S \cdot 9H_2O$ were used as precursor for the synthesis of $CuCdS_2$ nanoparticles in FNBR matrix. The optimum pH was determined for the nucleation, and the growth of the particles was carried at 3, 5 and 15 cycles. The obtained nanocomposite samples were named as $CuCdS_2$/FNBR(3c), $CuCdS_2$/FNBR(5c), and $CuCdS_2$/FNBR(15c) according to the number of cycles.

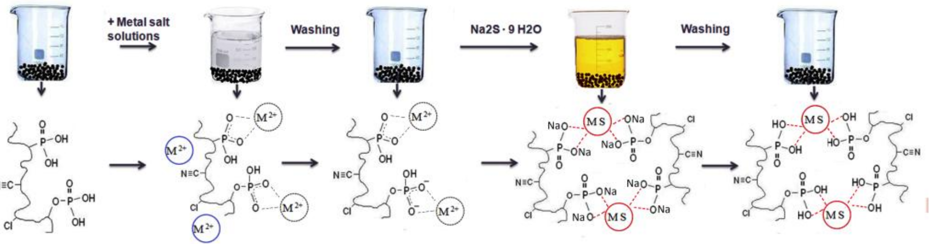

Figure 1. The formation process of metal sulfide nanoparticles in a FNBR polymer matrix using the SILAR method.

Application of ZnO- Al_2O_3/PVA nanocomposite to sorption of Pb^{2+} ions from aqueous solution. A 10^{-2} M $Pb(NO_3)_2$ solution was prepared and used to prepare working solutions. The concentration of Pb^{2+} ions in solution was determined by ICP-OES. Kinetics and thermodynamics of sorption were explained by studying the concentrations of ions at different temperatures and times. The mechanism of sorption was studied by Langmuir, Freundlich, Temkin and Dubinin-Radushkevich isotherm models.

Sorption and photocatalytic decomposition of dyes from aqueous solutions. The photocatalytic ability of nanocomposites synthesized in the presence of polymer and without polymer was studied by photodegradation of dye molecules under sunlight. Before the irradiation, sorption of dye molecules on the catalyst was carried out. At this time, the catalyst was kept in the dye solution in the dark for 1 day to reach the equilibrium. In order to accelerate the effective progress of photodegradation, the optimal pH was determined, doping, modification and intercalation of nanocomposites were carried out.

Research methods and technology. Scanning electron microscope (SEM), Transmission electron microscope (TEM), X-ray diffractometer (XRD), ultraviolet (UV) spectroscopy, infrared (IR) spectroscopy, electron paramagnetic resonance (EPR), Brunauer-Emmet-Teller (BET) analysis, thermogravimetric analysis (TGA), photoluminescence (PL) spectroscopy, optical emission spectroscopy (ICP-OES) were used to analyse the obtained nanomaterials.

In the third chapter, the analysis of the synthesized LDHs and their polymer nanocomposites was carried out. The discussion of the obtained results was justified and explained in detail, structure-property-size relationships were studied, physical-chemical regularities were investigated.

CoCr- LDH, α- and β- Co*($Co(OH)_2$) *and amorphous* $Cr(OH)_3$*: synthesis, modification and study. The XRD results of LDHs obtained at different temperatures, pHs and by different methods are shown in **Figure** 2. Peaks corresponding to hydrotalcite-like crystal structures are in (003), (006), (009), (012) (110) Miller planes and at 2θ =11.86°, 23.1°, 34.13°, 38.76°, 60.34° angles (JCPDS 38-0487)[3] was observed.

---

[3] Dinari, M. Structural, thermal and mechanical properties of polymer nanocomposites based on organosoluble polyimide with naphthyl pendent group and layered double hydroxide / M. Dinari, A.R. Rajabi // High Performance Polymers, - 2017. 29(8), - p. 951–959. DOI.org/10.1177/0954008316665678

The basal space of CoCr-LDH increased from 7.366 Å to 7.428 Å and 25.214 Å, after the interaction with SA and NaSt, respectively (Table 1). α- and β- Co(OH)2 were obtained along with LDH (**Figure 2**) at pH 7. A sharp difference in the amount of Co^{2+} and Cr^{3+} ions led to the formation of α-, β- $Co(OH)_2$ and amorphous $Cr(OH)_3$ in the reaction medium. With the decrease of Co^{2+} ions, the number of peaks of β-$Co(OH)_2$ increased. Amorphous $Cr(OH)_3$ was obtained when Co^{2+}:Cr^{3+} is 1:3 and 1:5.

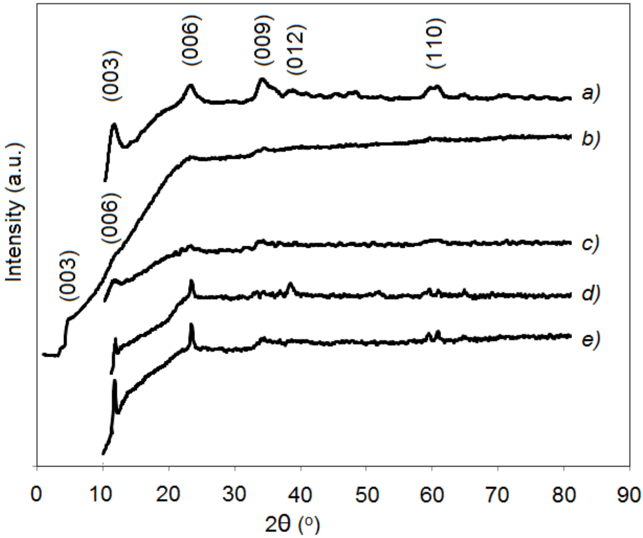

Figure 2. XRD results of a) CoCr-LDH$_{0.6M,\ 90°C}$, b) CoCr-LDH$_{0.6M,\ 90°C\ –\ NaSt}$, c) CoCr-LDH$_{0.6M,\ 90°C\ –SA}$, d) CoCr-LDH$_{20M,\ 90\ °C}$, e) CoCr-LDH$_{10M,\ 90°C}$ nanocomposites.

As can be seen from **Table 1**, the basal space calculated according to the (003) plane increased in the CoCr-LDH$_{10M,90°C}$ sample and decreased in the CoCr-LDH$_{20M90°C}$ sample. This is explained by the structural change in the highly concentrated basic solution. In a highly concentrated base solution, the system could not immediately reach its stable state, the average particle size was big in the samples obtained with 10M and 20M NaOH solutions. However, after heating the solution at 90°C, $Na_3[Cr(OH)_6$ was decomposed and because the concentration of NaOH in the solution was high, amorphous $Cr(OH)_3$

and CoCr-LDH were obtained which can be shown by the following reaction:.

$$Cr(NO_3)_3 \cdot 9H_2O + 6NaOH \rightarrow Na_3[Cr(OH)_6] + 3NaNO_3 + 9H_2O$$

$$Co(NO_3)_2 \cdot 6H_2O + 4NaOH \rightarrow Na_2[Co(OH)_4] + 2NaNO_3 + 6H_2O$$

$$Na_3[Cr(OH)_6] \rightarrow Cr(OH)_3 + 3NaOH$$

Table 1. Lattice parameters of CoCr-LDH nanostructures synthesized in different reaction parameters.

Parameters (Å)	CoCr-LDH $_{0.6M(25°C)}$	CoCr-LDH $_{0.6M\ 90°C)}$	CoCr-LDH $_{0.6M(90°C)}$-SA	CoCr-LDH $_{0.6M\ (90°C)}$- $_{NaSt}$
$d_{(003)}$	7.490	7.459	7.428	25.214
$d_{(006)}$	3.789	3.821	3.813	19.186
$d_{(110)}$	1.551	1.532	1.532	1.540
$a=2d_{110}$	3.102	3.064	3.064	3.08
$c=3d_{003}$	22.470	22.377	22.284	105.891
D (nm)	37.9	41.7	33.4	27.7

The formation of CoCr-LDH can be shown by the following reaction:

$$3Co(NO_3)_2 \cdot 6H_2O + Cr(NO_3)_3 \cdot 9H_2O + 6NaOH \rightarrow$$
$$\rightarrow Co_3Cr[(OH)_6]^{+3} \cdot 3(NO_3)^{-} \cdot y\ H_2O + 6NaNO_3$$

The surface morphology of CoCr-LDH$_{0.6M,90°C/NaSt}$ and CoCr-LDH$_{0.6M,90°C}$ samples was studied by TEM and SEM. The element composition was studied by EDX. By SEM analysis, the average particle size was about 100-150 nm and 30-50 nm in CoCr-LDH$_{0.6M,90°C}$ and CoCr-LDH$_{0.6M,90°C\ /NaSt}$ samples, respectively.

Organic groups caused a decrease in particle size and expansion of the layers after the modification. It is also clear that the size of the particles is big. In the case of intercalation of CoCr-LDH (**Figure 3c,d**), it is clear that the layers decrease and the dispers distribution increases. In the CoCr-LDH$_{0.6M(90°C)/NaSt}$ sample, the atomic number of elements per unit surface (Co/Cr=4.6/1.7) is less compared to the CoCr-LDH$_{0.6M(90°C)}$ sample (Co/Cr=19.6/6.7) is related to the expansion of the structure and the increase of voids.

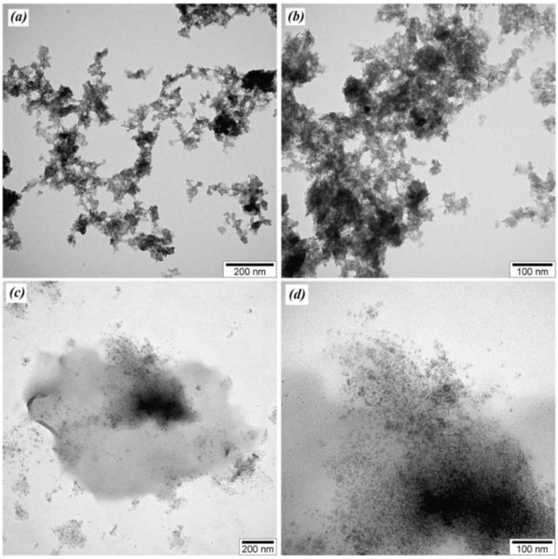

Figure 3. TEM image of as-synthesized (a, b) and intercalated (c, d) CoCr-LDH nanoparticles.

The results obtained by UV-Vis spectroscopy are shown in **Figure 4**.

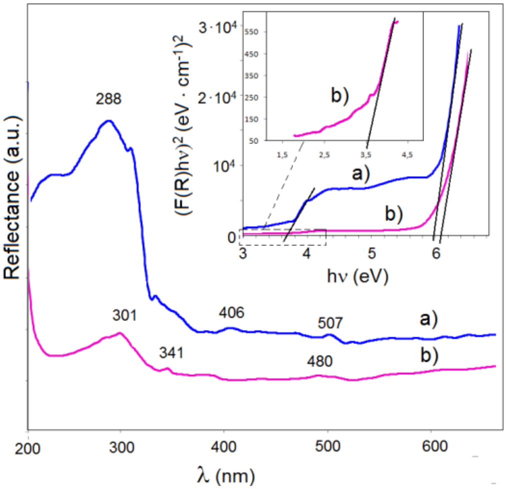

Figure 4. UV reflectance spectra and graphs of dependence of $[F(R\infty)h\nu]^2$ on hν.

Two bandgap values (E_g (high) and E_g(low)) were determined by extrapolating the straight part of the $[F(R\infty)h\nu]^2$ curves along the hν axes. The E_g (high) values of CoCr-$LDH_{0.6M(90°C)}$ and CoCr-$LDH_{0.6M(90°C)-NaSt}$ samples are 6.2 and 5.95 eV, and the E_g (low) values are 3.5 and 3.7 eV, respectively.

With increasing basal spacing, the gap of the electronic transition from the 2p-orbital of oxygen to the 4s or 3d of cobalt and chromium decreased, which is explained by the decrease in physical forces between the LDH layers.

Study of physicochemical properties of ZnAl-based LDH, oxide and mixed oxide nanomaterials depending on experimental parameters. A co-formation method was applied for the preparation of LDH/polymer nanocomposites. The XRD results of ZnAl-LDH_{2M}, ZnAl-LDH_{5M}, ZnAl-$LDH_{urea(2)}$ and ZnAl-mixed oxide/PVA nanocomposites are shown in **Figure** 5.

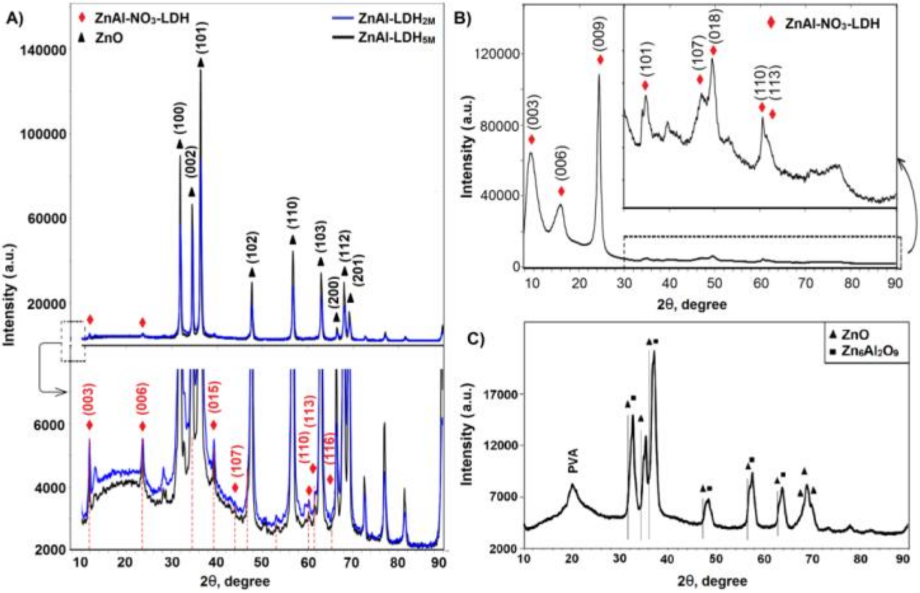

Figure 5. X-ray diffractograms of synthesized ZnAl-LDH nanoparticles and ZnAl-mixed oxide/PVA nanocomposites obtained by A) 2 M and 5 M NaOH B) urea, C) co-formation in 10% PVA/water solution.

2θ = 11.91° for ZnAl-LDH_{5M} and ZnAl-LDH_{2M}; 23.69°; 34.5°; 39.4°; 60.5° and 62.1° angles and (003) (006); (009); (015); (110)

and (113) Miller index planes confirm the characteristic peaks of hydrotalcite-like (HT) materials (JCPDS No.48-1023) with hexagonal crystal system. In the XRD results of ZnAl LDH_{5M} and ZnAl LDH_{2M} samples, the formation of the phase corresponding to ZnO at 2θ =31.9°, 34.57°; 36.4°; 47.7°; 56.76°; 62.99°; 66.45°; 68.05°; 69.19° angles and (002); (101); (102); (110); (103); (200); (112); (201) planes (JCPDS No. 89-7102) occurred due to the amphoteric nature of aluminum.

Optical properties of nanomaterials were studied using ultraviolet and infrared spectroscopy methods. Based on the infrared spectra of $ZnAlLDH_{2M}$, $ZnAlLDH_{5M}$, $ZnAlLDH_{urea(2)}$ and ZnAl-mixed oxide/PVA nanocomposites, the vibration of OH groups in the polyvinyl alcohol chain, LDH layers and interlayer water molecules was observed with a broad band in the range of 3415-3290 cm^{-1} in all samples. Absorption bands corresponding to NO_3^- groups with v3 intense vibration are observed at ~1363 cm-1 wave number in ZnAl LDH_{2M}, ZnAl LDH_{5M} and ZnAl-$LDH_{carb.(2)}$ samples. The 829 cm^{-1} and 752 cm^{-1} bands were also attributed to the presence of the NO_3^- group with D_{3h} symmetry[4]. This band was observed at a higher wave number (831 cm^{-1}) in the ZnAl-mixed oxide/PVA nanocomposite because the polymer chain enhances the vibration of free particles. However, since the interlayer distance in ZnAl-$LDH_{carb.}$ nanocomposite is wider than other samples ($d_{(003)}$ = 9.51 Å), that band fell to a lower wavenumber (752 cm^{-1}), and the mobility of NO_3^- ions was blocked by water molecules. The intense bands at 489, 509 and 536 cm^{-1} indicate the Zn-O-bonds belonging to the ZnO compound[5].

---

[4] Yang, F. Preparation and wettability of Zn–Al layered double hydroxide film directly grown on highly porous anodic alumina oxide template / F. Yang, B.Y. Xie, J.Z. Sun [et al.] // Materials Letters, - 2008. 62(8–9), - p. 1302–1304. DOI: 10.1016/j.matlet.2007.08.069

[5] Nagaraju, G. Electrochemical heavy metal detection, photocatalytic, photoluminescence, biodiesel production and antibacterial activities of Ag–ZnO nanomaterial / G. Nagaraju, S.A. Prashanth, M. Shastri [et al.] // Materials Research Bulletin, - 2017. 94, - p. 54–63. DOI.org/10.1016/j.materresbull.2017.05.043

Infrared spectroscopy analysis of ZnAl-mixed oxide/PVA-nanocomposite shows that the characteristic bands corresponding to OH, C-H, C = O, C-O and CH_2 groups are shifted from 3300, 2940, 1731, 1141 and 1420 cm-1 to the frequency of 3302, 2897, 1652, 1139 and 1411 cm-1, respectively. The shift towards lower frequency is explained by the formation of ZnAl mixed oxide nanoparticles in the PVA matrix. Since ZnAl mixed oxide nanoparticles are chemically attached to the PVS chain with the presence of these functional groups, the frequency and energy of these groups have decreased.

A very small amount of aluminum was involved in the reaction Energy-dispersive X-ray spectroscopy. The probable mechanism is shown as follows:

$$3Zn(NO_3)_2\cdot 6H_2O+Al(NO_3)_3\cdot 9H_2O+6NaOH\rightarrow$$

$$\rightarrow Zn_3Al[(OH)_6]^{+3}\cdot 3(NO_3^-)\cdot 9H_2O + 6NaNO_3$$

$$6Zn(NO_3)_2\cdot 6H_2O+2Al(NO_3)_3\cdot 9H_2O+18NaOH\rightarrow$$

$$\rightarrow Zn_6Al_2O_9\ (6ZnO+Al_2O_3) + 24H_2O + 18NaNO_3$$

When PVA was used in the experiment, the characteristic peaks of $Zn_6Al_2O_9$ belonging to cubic crystal phase was observed at $2\theta=$ 32.73°, 36.96(2)°; 37.26°; 48.27°; 57.51°; 63.77°; 68.79°, 70.08° and 78.0° diffraction angles (JCPDS No.51–0037). Nucleation proceeded before heating and small-sized hydrotalcites (ZnAl-LDH) were formed in the system along with ZnO nanoparticles using low-concentration of alkaline solution (2M NaOH).

SEM and EDX analysis of ZnAl-LDH_{2M} nanocrystals and ZnAl-mixed oxide/PVA nanocomposite are shown in **Figure 6** and it is observed that the particles are composed of rod-shaped and needle-shaped nanocrystals. The average length and width of the needles are 500-650 nm and 150-200 nm, respectively. During the formation of the nanocomposite, PVA formed a non-dispersed environment in the system, and the distribution of NaOH throughout the reaction was not homogeneous. Hexagonal morphology and big particles were formed (**Figure** 6B) without using polymer. The size of the particles was 1.5 μ - 500 nm by SEM. For both materials, the measurements obtained from XRD analysis are smaller than the measurements by

SEM. This is due to the aggregation of small crystallites to decrease the Gibbs free energy.

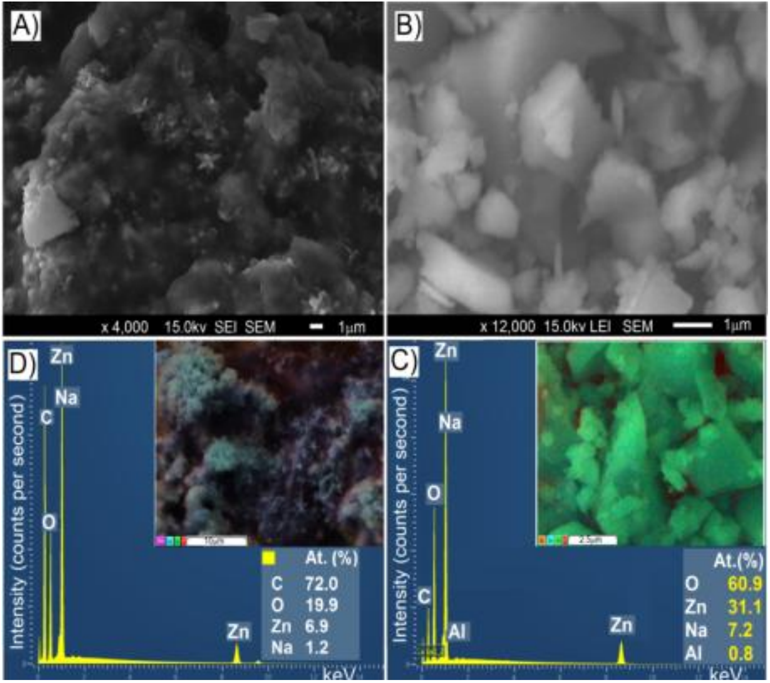

Figure 6. SEM images (A, B), EDX spectra (D, C) and elemental composition mapping of ZnAl LDH_{2M} nanocomposite synthesized with and without PVA.

According to UV analysis, $ZnAlLDH_{2M}$ and $ZnAlLDH_{5M}$ samples show three different bandgap values (E_g), which are indicated as E_{g1}, E_{g2}, and E_{g3} as high, medium, and low energy, respectively. The high bandgap value (E_{g1}) is related to the presence of NO_3^- anions in LDH [6].

---

[6] Ahmed, A. A. A. Zn–Al layered double hydroxide prepared at different molar ratios: Preparation, characterization, optical and dielectric properties / A.A.A. Ahmed, Z.A. Talib, M.Z. Bin Hussein [et al.] // Journal of Solid State Chemistry, - 2012. №191, - p. 271–278. DOI.org/10.1016/j.jssc.2012.03.013

E_{g2} and E_{g3} correspond to Me-O electron transition, which is observed for all samples. E_{g2}-values of ZnAl-LDH$_{2M}$, ZnAl-LDH$_{5M}$, ZnAl-LDH$_{urea(2)}$ and ZnAl-mixed oxide/PVA samples were estimated as 3.27, 3.17, 3.3 and 3.15 eV, respectively. Such low bandgap is promising in applications for photocatalytic devices, gas sensors, and photosensors.

Preparation of ZnAl-LDH/PVA nanocomposites. Zinc and aluminum containing LDH/PVA nanocomposites were prepared by applying co-formation and solution blending methods.

When the amount of the filler in the polymer is 0.05% and 0.1%, the substance-solution boundary in the samples was visible and the dispersed distribution was not complete. When the amount of filler in the polymer is 0.3%, the mixture turned into a white homogeneous solution after ultrasound. The diffraction peak at 2Θ = 19.17° corresponding to PVA shifted to a higher diffraction angle (2Θ = 20.00°) with the formation of ZnAl-LDH/PVA nanocomposite by co-formation metod (**Figure 7**). This case indicates the crosslinking of PVA by LDHs.

As the amount of LDH in the polymer increased, the wide band gap decreased slightly (E_{g1}=5.65eV) (Table 2). This is due to the penetration of the polymer solution into the LDH layers and the partial exclusion of anions from the interlayer space.

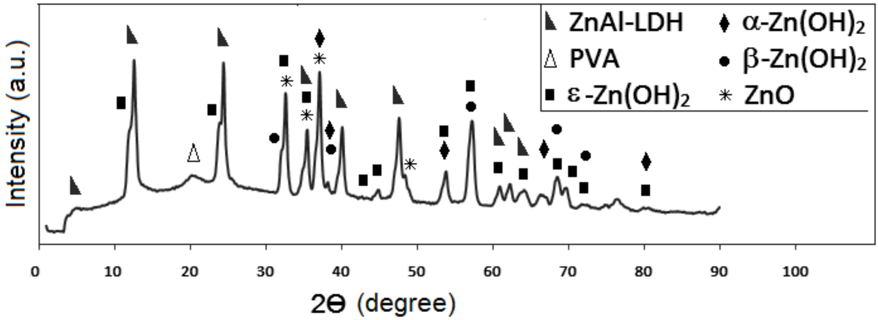

Figure 7. XRD analysis of ZnAl LDH/PVA nanocomposite.

Table 2. Band gap values calculated based on absorption and reflection bands of obtained nanocomposite.

The amount of ZnAlLDH-in PVA	E_g – from abs. (eV)			E_g - from reflec. (eV)		
	E_{g1}	E_{g2}	E_{g3}	E_{g1}	E_{g2}	E_{g3}
0.05%	6.22	5.95	1.60	4.50	3.90	2.00
0.1%	6.27	6.00	1.50	3.35	2.50	1.65
0.3%	5.65	4.70	3.65	3.25	2.70	1.70

Compared to 0.05% and 0.1% amounts of filler, the value of E_{g3} was high (3.65eV) for with 0.3% filler. This value corresponds to the quantum size effect and indicates that the size of the particles is further reduced. The intercalation has gone and the transition energy of the electron has increased with the inclusion of PVA in the layers of LDHs.

In chapter IV, the properties of doped LDHs with different metals and fullerene were characterized and the obtained results were discussed in detail.

Investigation of the properties of fullerene-doped LDHs and discussion of the obtained results. Füllerene (C_{60}) was non-covalently added to ZnAl-LDH/PVA nanocomposites and the obtained samples were applied to the photodegradation of dye molecules. XRD results of 1, 10, 20, 60% C_{60} doped and pure ZnAl-LDH/PVA nanocomposites are shown in **Figures 8**.

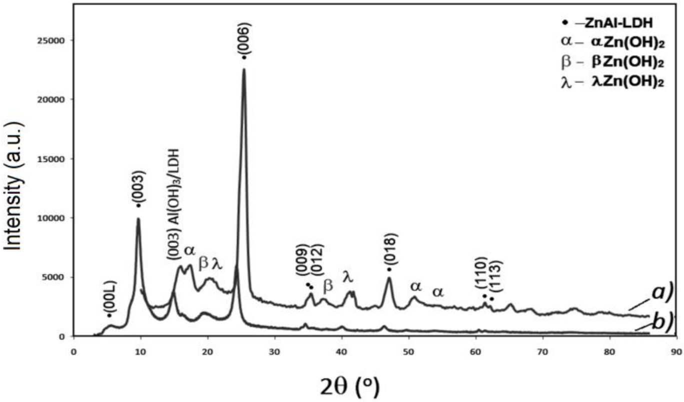

Figure 8. XRD patterns of the as-synthesized (a) and 1% C_{60} (b) doped ZnAl-LDH/PVA nanocomposite.

The peaks corresponding to (003); (006); (009); (012) and (110) Miller index planes (JCPDS file 38-0487) were observed at 2θ = 9.5; 24.14; 34,32; 39.26; at 60 and 61° degrees for 1% C60 doped and at 2θ = 10.2; 24.63; 35,37; 41.24; 60 and 61° degrees for pure ZnAl-LDH/PVA nanocomposite. Crystals obtained by uniform deformation model (VDM) were assumed to be isotropic in nature. But since doped structures have defects and distortions in the crystal lattice, they also have an anisotropic nature.

As can be seen from the SEM image of the samples, a rice-shaped nanoparticles with a width of 150 nm-1000 nm and a length of 0.4 μm-20 μm were formed (**Figure 9**). However, the surface morphology of nanoparticles is closer to spherical structure according to TEM results, the formation of LDH nanoparticles took place in the polymer matrix and the particles combined to form agglomerates and resulted in polydispersity by SEM images.

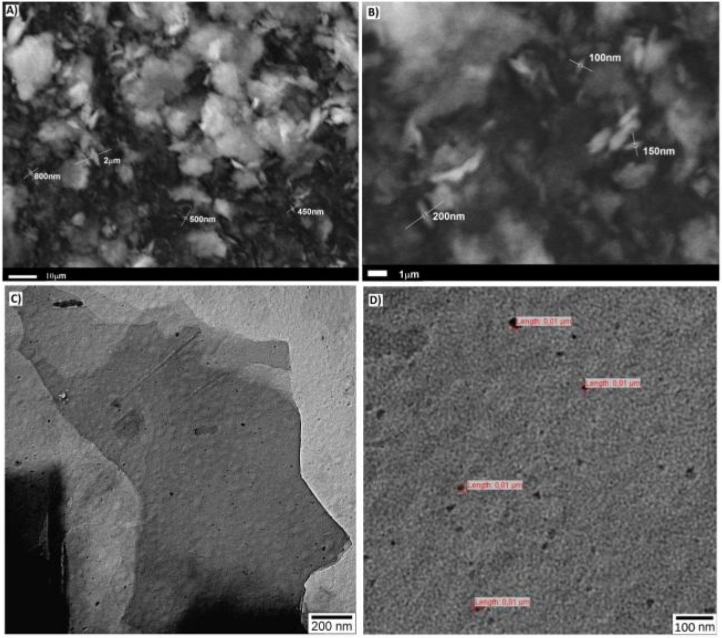

Figure 10. SEM (A, B) and TEM (C, D) images of the ZnAl-LDH/PVA nanocomposite doped with 60% C_{60}.

A red shift occurred in the absorption spectra of the nanocomposite doped with C_{60}. As the amount of C_{60} increased, the red shift changed to a blue shift, and this situation was also observed in previous works. The red and blue shifts in the absorption spectra are explained by the Urbach energy (E_U) and the Burstein-Moss effect, respectively. As the amount of C_{60} in the nanocomposite varied from 0% < 1% < 60% < 20% < 10%, E_g decreased and E_U increased. The highest value of E_U occurred as a result of doping with 10% C_{60}, which is associated with more defects in the crystal lattice (**Table 3**).

Table 3. E_g and E_U of C_{60} doped ZnAl-LDH/PVA.

Samples	$E_{g(indirect)}$ (eV)	$E_{g(direct)}$ (eV)	E_u(eV)
ZnAl-LDH/PVA	3.75	2.34	0.1343
1% C_{60}/ZnAl-LDH/PVA	2.85	1.87	0.1623
10%C_{60}/ZnAl-LDH/PVA	2.90	1.56	0.5998
20%C_{60}/ZnAl-LDH/PVA	3.02	1.61	0.2592
60%C_{60}/ZnAl-LDH/PVA	2.80	1.42	0.2296

PL spectra of PVA, Zn-Al LDH/PVA and 1% C_{60} doped ZnAl LDH/PVA nanocomposites are shown in **Figure** 11.

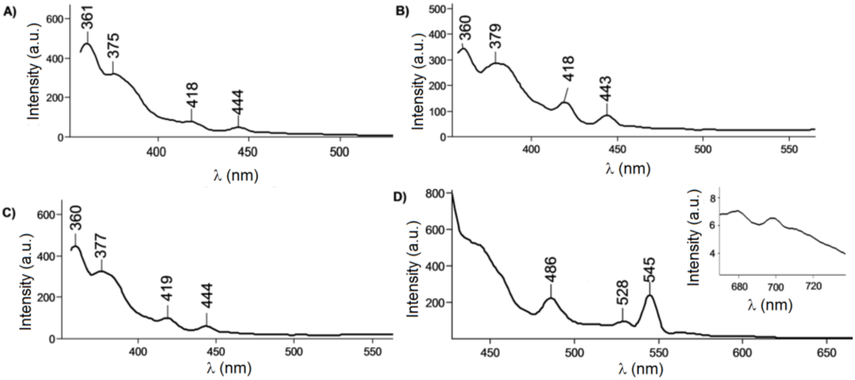

Figure 10. PL spectra of PVA (A), Zn-Al LDH/PVA (B) and C_{60} doped ZnAl LDH/PVA (C,D) nanocomposites taken at 325 nm (A-C) and 400 nm (D) excitation energy.

With the increase of components in the composition of the nanocomposite, the intensity of the emission bands increased, oxygen vacancy and intermediate types of zinc (Zn interstitial: Zn_i^{++}, Zn_i^{+}, Zn_i*) were formed with deep-level defects. The bands observed at 545 nm and 700 nm wavelengths in the spectrum of C_{60}-doped ZnAl-LDH/PVA nanocomposite correspond to C_{60}, and these bands were observed at 500 and 750 nm in the PL spectra of pure C_{60} with excitation at 302 nm.

In chapter V, the properties of metal sulfide/polymer nanocomposites obtained on the basis of FNBR and LDH were studied and the results were discussed.

Study of physicochemical properties of CdS, ZnS and $CdZnS_2$ nanomaterials synthesized on the basis of FNBR.

XRD results of CdS/FNBR, $Cd_{0.75}Zn_{0.25}S$/FNBR, $Cd_{0.5}Zn_{0.5}S$/FNBR, $Cd_{0.25}Zn_{0.75}S$/FNBR and ZnS/FNBR nanocomposites synthesized by SILAR method in 5 and 15 cycles are shown in **Figure 11**. The obtained nanocomposites were obtained with 3 intense peaks with (111), (220) and (311) Miller indices corresponding to the characteristic peaks of CdS (JCPDS#65-2887) and ZnS (JCPDS#39-1363) in the cubic phase. The average size of nanocrystallites was calculated by Scherrer (1) and Williamson-Hall (2) equations [7,8].

$$D = \frac{K\lambda}{\beta_{hkl}cos\theta} \quad (1) \qquad \beta_{hkl}cos\theta = \frac{K\lambda}{D} + 4\varepsilon sin\theta \quad (2)$$

The formation of ternary sulfides was observed by the shift of diffraction peaks. The calculated Young's modul of CdS and ZnS nanoparticles in (111), (220) and (311) planes are 97.84, 78.51; 64.33 m^2/N and 95.84; 69.68; is 53.42 m^2/N respectively. Since CdS is assumed to be the dominant structure, the geometric parameters of $CdZnS_2$ ternary sulfide nanoparticles were calculated using the Young's modulus of cubic CdS.

---

[7] Scherrer, P., Nachrichten von der Gesellschaft der Wissenschaften zu Göttingen, Mathematisch–Physikalische Klasse,1918 (1918) 98–100

[8] Mote, V., Purushotham, Y. & Dole, B. Williamson-Hall analysis in estimation of lattice strain in nanometer-sized ZnO particles. J Theor Appl Phys 6, 6 (2012). https://doi.org/10.1186/2251-7235-6-6

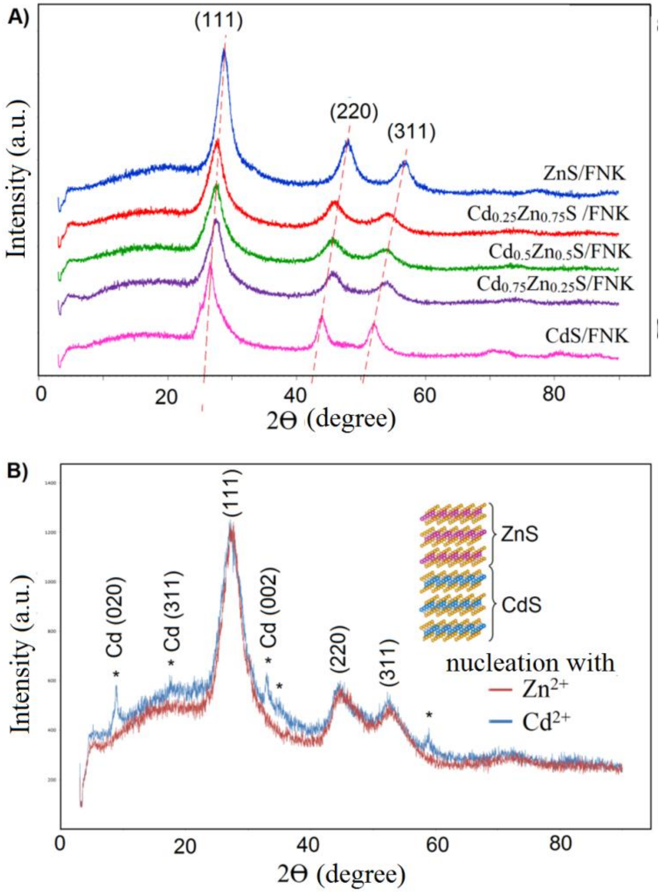

Figure 11. XRD patterns of $CdZnS_2$ nanoparticles obtained from A) Mixed solution and B) Sequential synthesis at 15 cycles.

The mechanism of nanoparticle formation was explained by IR spectroscopy. IR spectra of nanoparticles synthesized in FNBR and activated carbon (AC) matrix (for comparison) are presented in **Figure 12**. the characteristic bands of -OH (3429 cm^{-1}), C–H (2918 cm^{-1}), P–O–H (2864 cm^{-1}), $OPO(OH)_2$ (2000-2200 cm^{-1}) and P = O (1552 cm^{-1}) correspond to FNBR. The bands corresponding to PO_3^{2-} (977 cm^{-1}) group shifted to 969 cm^{-1}, 975 cm^{-1}, 972 cm^{-1}, 973 cm^{-1} and 972 cm^{-1} frequency with the formation of CdS, ZnS, $Cd_{0.5}Zn_{0.5}S$, $Cd_{0.75}Zn_{0.25}S$ and $Cd_{0.25}Zn_{0.75}S$ nanoparticles. The red shift in the IR spectrum shows that nanoparticles coordinated to functional groups have weakened the movement of the polymer chain. The possible mechanism of the synthesis of sulfide nanoparticles in the functional groups of FNBR can be shown by the following reactions:

Adsorption of the cations:

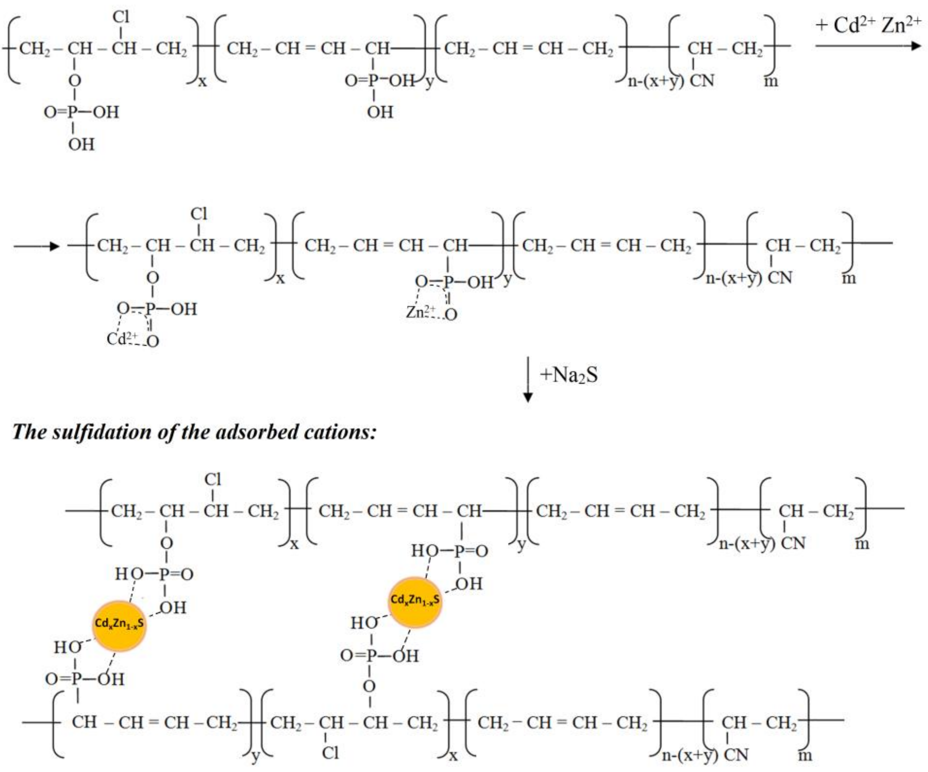

The sulfidation of the adsorbed cations:

General grows of cadmium zinc sulfide nanocrystals:

$Cd^{2+} + Zn^{+} + S^{2-} \rightarrow Cd_xZn_{1-x}S$ (x=1; 0; 0.25; 0.5 and 0.75)

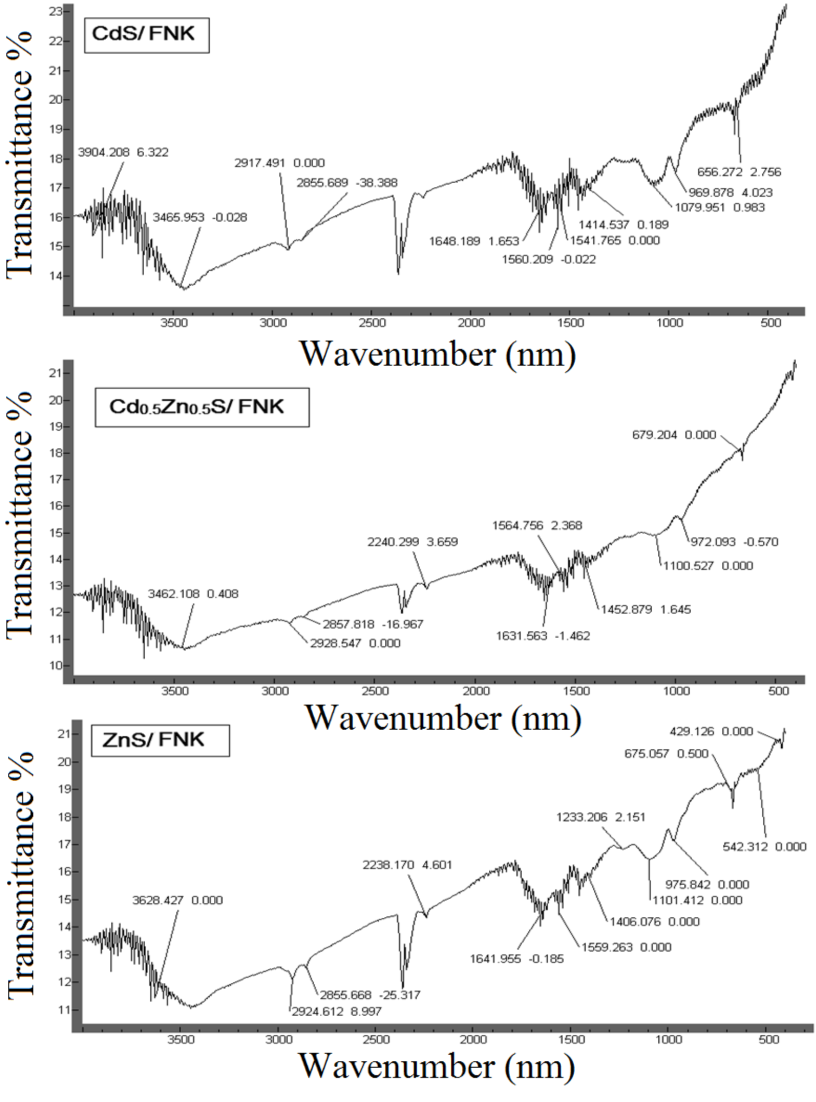

Figure 12. Infrared spectra of $Cd_xZn_{1-x}S$/FNBR and $Cd_{0.5}Zn_{0.5}S$/AC nanocomposites

The thermal properties of raw (BNK), modified (FNBR) and FNBR containing metal ions (Cd^{2+} and Zn^{2+}) were studied at a temperature of 20-900 ºC at a heating rate of 10 ºC/min, TQ and DTQ curves were obtained (**Figure 13**).

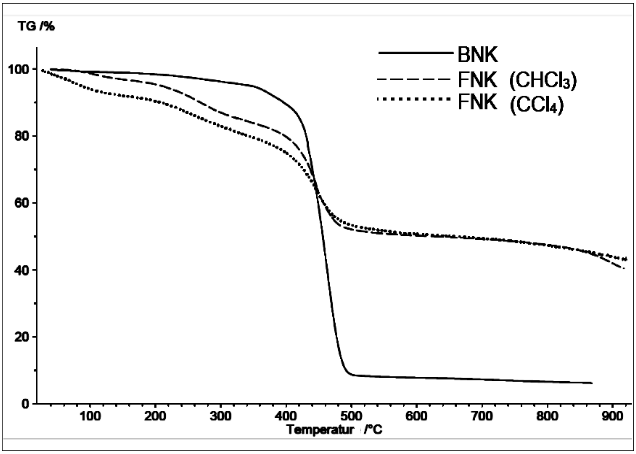

Figure 13. Thermogravimetric analysis of NBR and FNBR

One-stage decomposition occurred in the primary polymer (NBR), it lost 89% of its total mass at 350-400°C, and 92.8% at 600 ºC. FNBR and metal ions (Cd^{2+} and Zn^{2+}) containing FNBR underwent a three-step thermal decomposition. The initial mass loss is due to evaporation of sorbed water. The mass loss in the second stage of thermal analysis indicates the condensation of phosphonic acid and the last third stage the decomposition of polymer chain (Scheme 1). The polymer composite showed significant thermal stability and its application as a stabilizer in the formation of nanoparticles is favorable. In the second stage of thermal analysis of FNBR, Cd^{2+}/FNBR and Zn^{2+}/FNBR, the mass loss at 446.5 °C, 444 °C and 438.8 °C was 45.03%, 42.52% and 39.9% of the total mass, respectively. The total mass loss of FNBR, Cd^{2+}/FNBR and Zn^{2+} /FNBR was 93.76, 59.77, 60.03 and 57.79% (**Scheme 1**).

The surface morphology of $Cd_{0.5}Zn_{0.5}S$/FNBR nanocomposite was studied by SEM and TEM, the average particle size is ~25-50 nm by SEM and ~10-20 nm by TEM. Cd, Zn, and S atomic ratios are 1.09/1/1.9, 1.3/1/2.13 and 1/1/1.77 in $Cd_{0.75}Zn_{0.25}S$, $Cd_{0.5}Zn_{0.5}S$, and $Cd_{0.25}Zn_{0.75}S$ ternary sulfide, respectively. Since the solubility product of CdS (Ksp = 8.0×10−27) is smaller than that of ZnS (Ksp = 1.6×10−12), the content of cadmium in ternary sulfides is high.

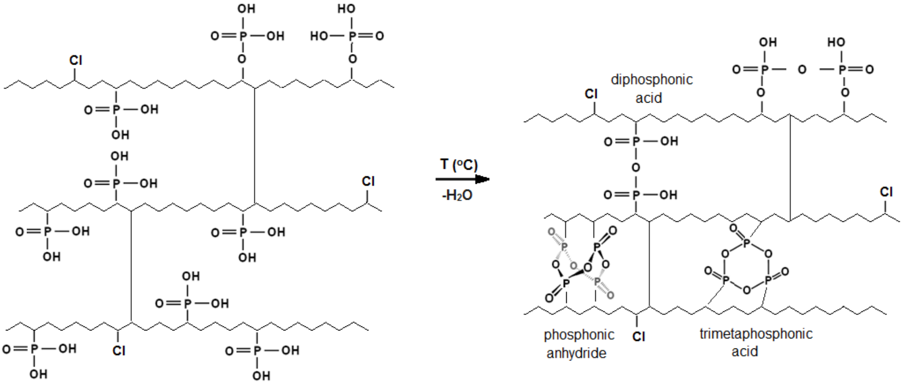

Scheme 1. Probable mechanism of the thermal analysis by condensation of phosphonic groups.

Study of physicochemical properties of CuS, CdS and $Cu_{0.5}Cd_{0.5}S$ nanomaterials synthesized on the basis of FNBR. In this work, SILAR synthesis and thermal annealing of copper cadmium sulfide/polymer nanocomposites was carried out, and the formed new phases were associated with the size-structure-property effects.

Figure 14 shows the XRD patterns of $Cu_xCd_{1-x}S$/FNBR synthesized at different reaction times and SILAR cycles. In the compound $Cu_xCd_{1-x}S$, when "x" = 1 and 0, good crystallization was observed, and pure binary sulfides were formed. The low intensity peak observed at 2Θ = 20° diffraction angle corresponds to FNK.As can be seen from Figure 14, the $Cu_xCd_{1-x}S$ compound is dominated by strong diffraction peaks corresponding to cubic CdS (JCPDS 10-0454) at low periods of the SILAR method when x = 0.5, but 2Θ = 48.03° in the (107) Miller index plane. Only one peak (JCPDS 06-0464) corresponding to CuS is observed. The result of X-ray diffractograms of $Cu_{0.5}Cd_{0.5}S$/FNK nanocomposite shows that the diffraction pattern begins to correspond to CuS with increasing number of cycles. This compatibility is further refined by increasing the reaction time from 30 minutes to 24 hours. Diffraction peaks corresponding to CdS in 3 cycles and CuS in 15 cycles dominated and in the corresponding cycles, the crystal lattice of binary sulfides was dominant. This situation was explained by supersaturation and chemical potential. The nucleation rate is greater at high level supersaturation, than the crystal growth rate. Here, at supersaturation, the increase of nucleation centers prevailed and resulted in smaller crystallites. This supersaturation dominates the nucleation. Some new and relatively intense peaks corresponding to crystalline phases of copper sulfide ($Cu_{2-x}S$ and Cu_2S) formed during 15 cycles of the SILAR method are related to the crystallization time and the number of cycles.

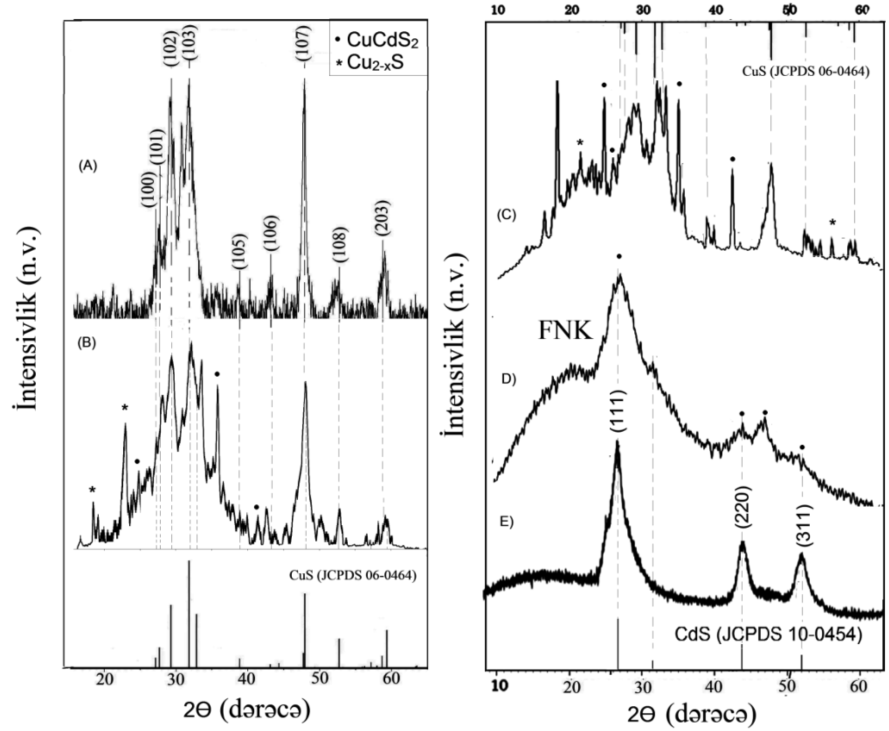

Figure 16. X-ray diffractograms of (A) CuS (15 cycles), (B) $Cu_{0.5}Cd_{0.5}S$ (15 cycles), (C) $Cu_{0.5}Cd_{0.5}S$ (t = 30 min, 15 cycles), (D) $Cu_{0.5}Cd_{0.5}S$ (t = 30 min, 5 cycles) and (E) CdS (t = 24h, 15 cycles) nanocomposites synthesized on the basis of FNBR.

The Raman spectrum of the $Cu_{0.5}Cd_{0.5}S$/FNBR nanocomposite shown in **Figure 15** reflects the agreement with the interpretation of the results obtained by XRD. Optical Raman spectrum of $Cu_{0.5}Cd_{0.5}S$/FNBR nanocomposite is observed with six peaks at 262, 405, 593, 714, 999 and 1100 cm^{-1} wavenumbers. The intense peaks at 262, 405, and 714 cm−1 wave numbers correspond to the phonon mode (1LO), the first (2LO) and the second (3LO) overtone of $Cu_{0.5}Cd_{0.5}S$, which is in agreement to the peaks of the Raman spectrum of copper sulfide with a red shift (**Table 4**).

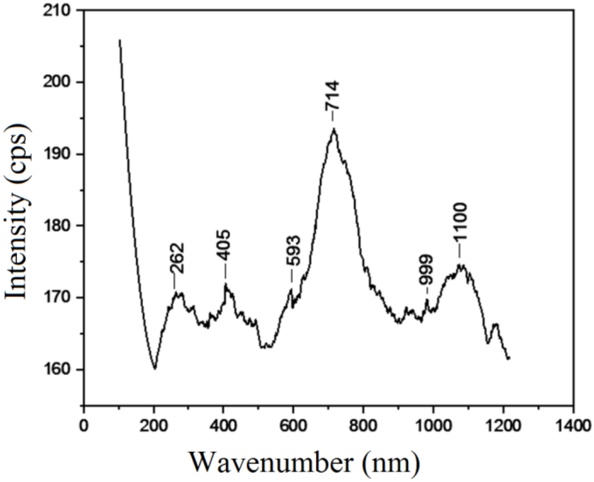

Figure 15. Raman spectrum of $Cu_{0.5}Cd_{0.5}S$/FNBR nanocomposite.

Table 4. Evaluation of peaks of synthesized $Cu_{0.5}Cd_{0.5}S$/FNBR in15 cycles according to X-ray diffraction and Raman spectrum results.

$Cu_xCd_{1-x}S$	D (nm)	1LO	2LO	3LO	References
x= 0.5	7.39	262	405	714	In this work
x = 1	9.09	265	474	-	[9]
x = 0	3.2	300	600	900	[10]

---

[9] Chaki, S. H.; Tailor, J. P.; Deshpande, M. P. Covellite CuS - Single Crystal Growth by Chemical Vapour Transport (CVT) Technique and Characterization. Mater. Sci. Semicond. Process., 2014, 27 (1), 577–585.

The results of the study of $Cu_{0.5}Cd_{0.5}S$/FNBR by SEM, TEM and EDS are given in **Figure 16**.

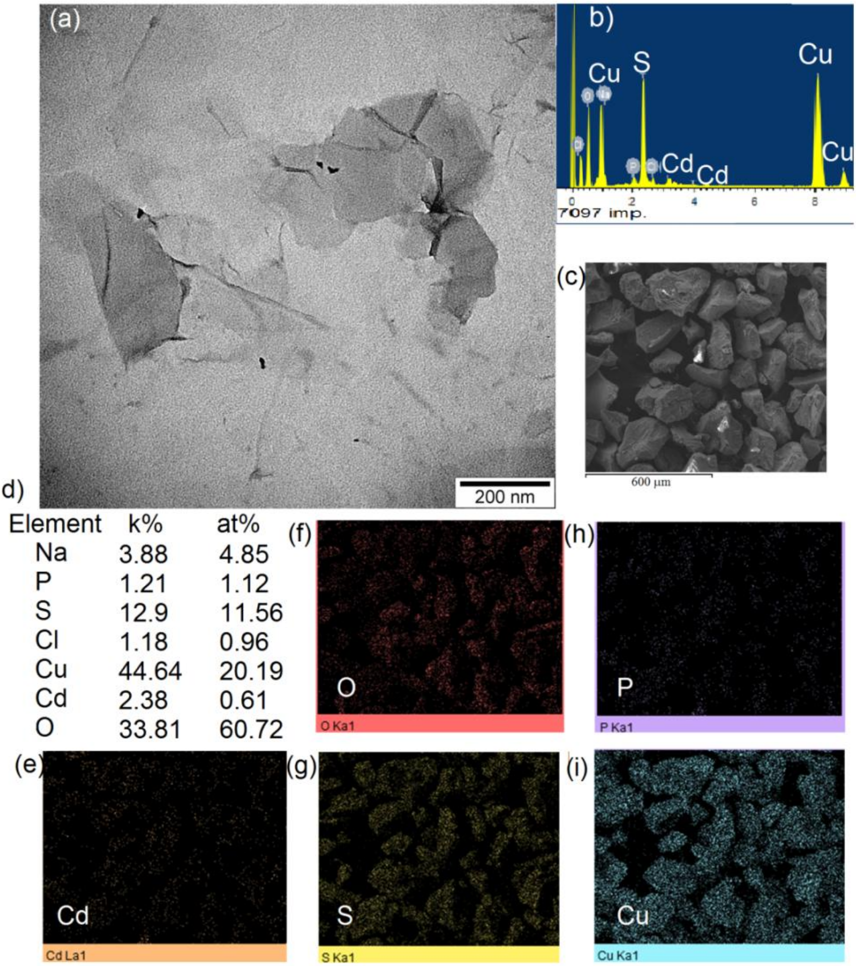

Element	k%	at%
Na	3.88	4.85
P	1.21	1.12
S	12.9	11.56
Cl	1.18	0.96
Cu	44.64	20.19
Cd	2.38	0.61
O	33.81	60.72

Figure 16. TEM (a), SEM (b, c) and EDS (e-j) results of $CuCdS_2$/FNBR nanocomposites.

---

[10] Kumar, P.; Saxena, N.; Chandra, R.; Gua, V.; Agarwal, A.; Kanjilal, D. Nanotwinning and Structural Phase Transition in CdS Quantum Dots. Nanoscale Res. Lett., 2012, 7, 1–7. https://doi.org/10.1186/1556-276X-7-584.

The average size of the particles by TEM is 20-30 nm. Although the initial concentrations of Cu^{2+} and Cd^{2+} ions in the solution were taken in a molar ratio of 1:1, the atomic percentage in ternary sulfide was 20.19% and 0.61%, respectively. This is in good agreement with XRD results. It is known that the rate of nucleation and sulphidation is different for each substance. Formation of primary crystals and high supersaturation are important to ensure proper nucleation and co-precipitation rates. The solubility products of Cu+, Cu^{2+} and Cd^{2+} sulfides are Ksp = 2.5 x 10-48, 1.69 x 10-36 and 8.0×10-27 at 25°C, respectively. For multicomponents, the activity-based supersaturation ratio and chemical potential difference ($\Delta\mu$) increase with increasing Ksp. This leads to a high degree of supersaturation where the nucleation rate is increased, which dominates the crystal growth.

Since the $CuCdS_2$ crystal lattice contains both Cd and Cu atoms, its bandgap may be different from that of CuS and CdS. The bandgap varies in the order of 1.42-2.36 eV in $CuCdS_2$ bulk structures.

Here, the wide bandgap (~3.7 eV) is explained by the formation of nanoparticles in the limited volume of FNBR (**Figure 17**). Bulk $Cu_{0.5}Cd_{0.5}S$ has a bandgap about 2.4 eV and is a p-type semiconductor. Knowing that the binary sulfides of Cd and Cu metals are sensitive to light and are applied in many fields such as photoelectrics, sensors, thermal agents, their application in photocatalysis is also inevitable.

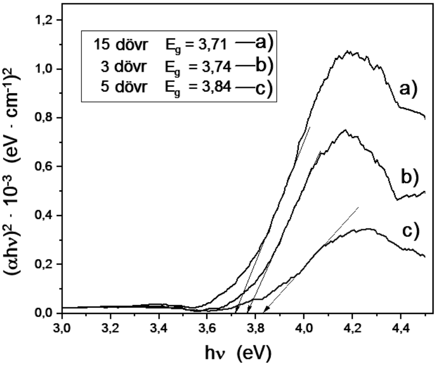

Figure 17. Tauc plots of $Cu_{0.5}Cd_{0.5}S$/FNBR nanocomposite obtained at 3 (a), 5 (b) and 15 (c) cycles. A) Direct bandgap; B) Indirect bandgap.

The dielectric properties of the $CuCdS_2$/FNBR nanocomposite were studied by using E7-20" (MNIPI) (Belarus) device at 25, 40, 60, 80, 100 and 120°C in an electric field varying from 10^2 to 10^6 Hs. CuCdS2/FNK nanocomposite was finely ground and mixed with an aqueous solution of polyvinyl alcohol (5%), formed into a thin film and dried. Measurements were made between metal electrodes by placing copper plates on both sides of the obtained layer. The changes and regularities of dielectric parameters (dielectric constant (ε'), dielectric loss (ε" and tgδ), conductivity (σ), dielectric modulus (M' and M"), etc.) were studied at low, medium and high frequencies, at different temperatures to assess interfacial, dipole-dipole and ionic interactions. The dielectric constant of the $CuCdS_2$/FNBR nanocomposite (**Figure 18**) is lower than that of CuS/FNBR at room temperature. Also, the dielectric constant (ε') of $CuCdS_2$/FNBR nanocomposite increased intensively with increasing temperature, in which case the nanoparticles are dispersed in the polymer matrix and the interfacial interaction is intense at all temperatures.

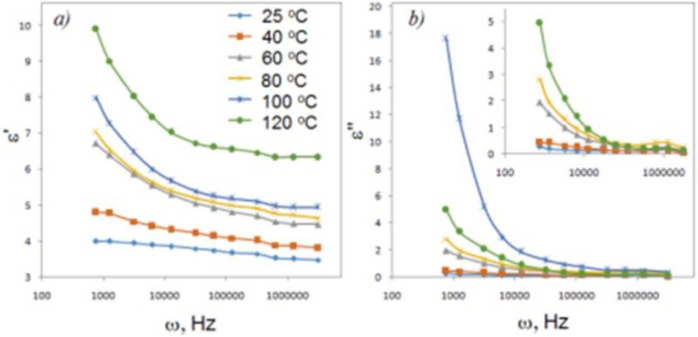

Figure 18. Frequency dependence of dielectric constant (a) and dielectric loss of $CuCdS_2$/FNBR.

Dielectric loss (ε") of CuS/FNBR nanocomposite measured at room temperature is higher than $CuCdS_2$/FNBR. A high value of ε" increases the potential ability of the dielectric material to use it at less energy consumption. The Cole-Cole curves of CuS/FNBR at room temperature and $CuCdS_2$/FNBR at different temperatures show that a well formed Cole-Cole arc was observed because the CuS/FNBR sample contained only binary sulfide.

The EPR spectra of CuS/FNBR, CdS/FNBR and $Cu_{0.5}Cd_{0.5}S$/FNBR nanocomposites were recorded at room temperature and shown in **Figure 19**. EPR spectra of CuS/FNBR nanocomposite correspond to Cu^{2+} ions and EPR has central axial symmetry ($g_x = g_y < g_z$). The intensity of the EPR spectrum is 1.8×10^6 for $Cu_{0.5}Cd_{0.5}S$ and 2.5×10^4 for CdS. 72 times lower intensity of EPR spectrum of CdS proves that g_3 belongs to copper and but to cadmium, and the center of symmetry is orthorhombic.

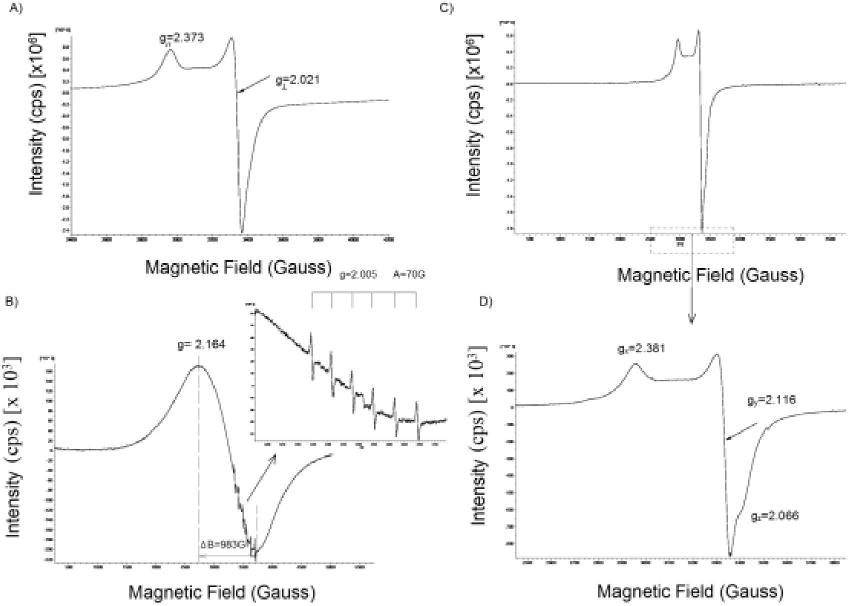

Figure 19. Electron paramagnetic resonance spectra of CuS/FNBR, CdS/FNBR and $CuCdS_2$/FNBR nanocomposites.

$CuCdS_2$/FNBR nanocomposite was heated at 150, 250, 350, 450, 550 and 700 °C in air, and a phase transformations and oxidation of ternary sulfide were studied. The binary sulfides of the metals that make up this compound, CuS is completely converted to CuO by thermal annealing in air, but CdS is not completely converted to CdO, it forms sulfates. The conversion of $CuCdS_2$ to $CuCdO_2$ by heating in air is not available on XRD PDF cards. The peaks obtained when $CuCdS_2$/FNBR was heated at 700°C closely matched to CuO, but all peaks were observed at a slightly lower diffraction angle. Peaks belonging to CuO at 35.74°, 38.95°, 49.2°, 53.88°, 58.76°, 61.79°, 66.22°, 68.42°, 72.67°, 75.37°, 83.21° 35.07°, 38.22° angles were observed at 48.31°, 53.05°, 57.84°, 61.11°, 65.37°, 67.68°, 72.02°, 74.86°, 82.78° after heating CuCdS2/FNBR nanocomposite at 700°C. Due to the influence of temperature, a change of lattice parameters occurred before oxidation with the entering of oxygen into the crystal lattice.

Research and analysis of the properties of CdZnS/CdZnAl-LDH/PVA nanocomposites obtained on the basis of CdZnAl LDH/PVA nanocomposite**.** In this study, a CdZnS-modified CdZnAl-LDH/PVA nanocomposite with ionic and electronic conductivity, was synthesized and applied to the photodegradation a very harmful organic pollutant of m-cresol from water. The intensity of the peaks corresponding to LDHs decreased, and new peaks were formed corresponding to cadmium and zinc ternary sulfides ($CdZnS_2$) obtained by the direct sulphidation of LDHs at room temperature and 40°C. The average particle size of $CdZnS_2$ nanocrystallites in CdZnAl-LDH/PVA and $CdZnS_2$/CdZnAl-LDH/PVA nanocomposites obtained at 25°C and 40°C is 14.25 nm, 19.05 nm and 16.5 nm, respectively. A red shift was observed in the UV-Vis absorption spectra of $CdZnS_2$-LDH/PVA nanocomposites after the sulfidation. The bandgap of CdZnAl-LDH/PVA nanocomposite decreased from 2.75 eV to 2.6 eV and 2.55 eV after the sulfidation at 25°C and 40°C, respectively.

In chapter VI, the application of obtained nanocomposites to sorption and their regularies are discussed.

Sorption of Pb^{2+} ions by ZnO-Al_2O_3/PVA nanocomposite from aqueous solution. The sorption of Pb^{2+} ions on ZnAl mixed oxide/PVA nanocomposite increased with increasing pH from 3.0 to 5.0, then rapidly decreased to 8.0 and increased again at higher pH (**Figure 20**). In aqueous solutions, metal (Me) ions can exist in different forms, $Me^{2+} \rightleftharpoons Me(OH)^+ \rightleftharpoons Me(OH)_2 \rightleftharpoons Me(OH)_3$ - at different pH values. The optimum pH for the sorption of Pb^{2+} ions onto ZnAl mixed oxide/PVA nanocomposite was 5.

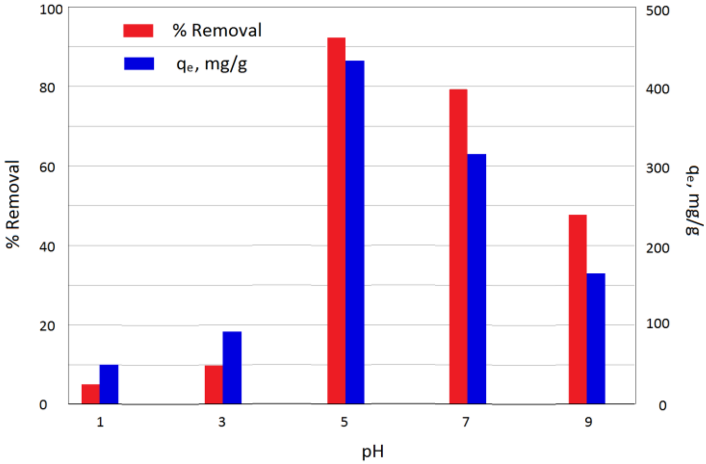

Figure 20 Effect of pH on the adsorption of Pb(II) on ZnAl mixed oxide /PVA nanocomposite (C_0 = 331.4 mg/l, T = 25 °C, t = 180 min).

Phase transitions at different pH value occurring in the structure of ZnO-Al_2O_3/PVA nanocomposite with the sorption of Pb^{2+} ions are shown in **Figure 21**. As can be seen, crystallization has occurred in the ZnO and $Zn_6Al_2O_9$ phases, which conform to ICDD #36–1451 and ICDD #51–0037 standards, respectively. In Pb^{2+} ions sorbed ZnAl mixed oxide/PVA nanocomposite material, the diffraction peaks belonging to $Zn_6Al_2O_9$ disappeared at different pH and a new compound with $Pb_3(CO_3)_2(OH)_2$ composition (ICDD: 00-013-0131) was formed. By increasing the pH value, chemical sorption prevailed, and isomorphous substitution increased. Pb^{2+} ions were involved in the formation of aqua-, hydroxyl- and ammonium- $[Me(NH_3)^{2+}]$ complexes in the solution with a pH 3 to 10, and the amount of complexes in the solution was different at different pH[11]. The main types of lead ions at the studied pH are Pb(II), PbOH+, $Pb_4(OH)_4^{4+}$ and $Pb_3(OH)_4^{2+}$.

---

[11] Alosmanov, R.M. Sorption of some heavy metals ions by phosphorus–containing polymer sorbent in dependence from medium acidity / A.A. Azizov, A.M. Maharramov, I.A.Bunyad–Zadeh // Journal of International Environmental Application and Science., 2011, v.6, No.3, - p. 448–451

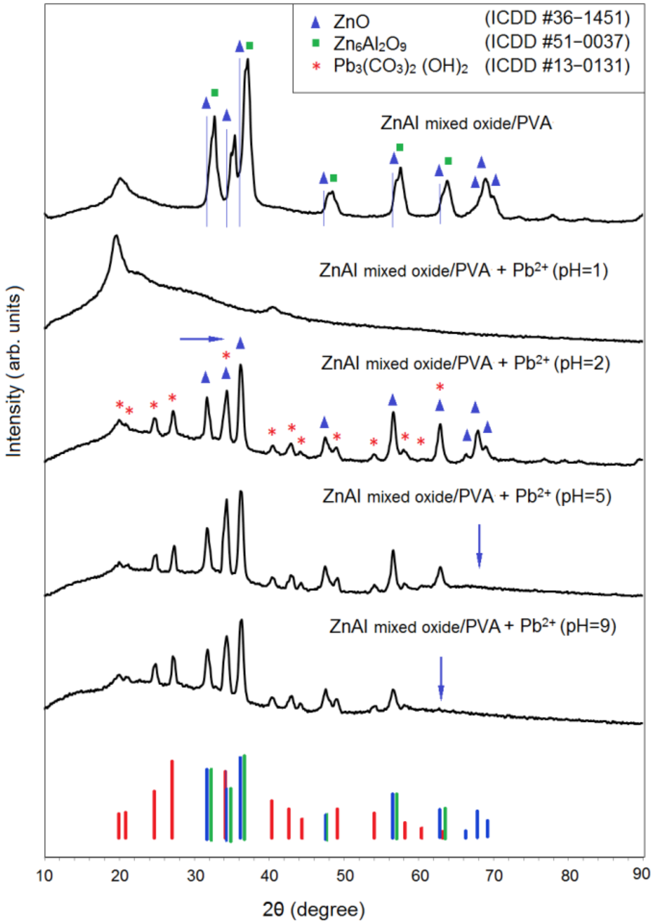

Figure 21. X-ray diffractograms of Pb^{2+} ions sorbed ZnAl mixed oxide/PVA nanocomposite at different pH.

It was observed that the bandgap of nanocomposite decreased in all materials used in the sorption at high pH solution. Since sorption occurs with the formation of variable complexes (PbZnAl- mixed oxide, $PbOH^+$, $Pb_4(OH)_4^{4+}$, $Pb_3(OH)_4^{2+}$, $[Pb(NH_3)^{2+}]$ and $Pb_3(CO_3)_2(OH)$, Pb^{2+} was entered into the composition with big ion radus

The degree of sorption (%) increased with increase of the amount of sorbent, and the optimum amount was chosen to be 5 g/l. The mechanism of sorption is explained according to the Freundlich isotherm model (**Table 5**):

Table 5. Isotherm parameters of the sorption of Pb^{2+} ions onto ZnAl mixed oxide/PVA nanocomposite at 298K.

Langmuir			Freundlich			D-R			
ST_{mak} mq/q	K_L, l/mq	R^2	n	K_F	R^2	β	ST_{tar}, mq/q	E, kJ/mol	R^2
1000	$6.13 \cdot 10^{-3}$	0.91	1.3	5.64	0.96	0.54	159.9	0.96	0.7

According to the Freundlich isotherm model: Means heterogeneous adsorption process; Sorption is not limited and occurs in many layers; Active centers are not equivalent and have different energy; Adsorbed particles can also act as active centers. Thus, sorption can continue even if the active centers are occupied. Physical adsorption occurred when the experiment was carried out at neutral pH, E = 0.964 kC/mol. The sorption of Pb^{2+} ions on ZnAl mixed oxide/PVA nanocomposite conformed to the pseudo-II-order kinetic model and the correlation coefficient (R^2) was high (**Table 6**).

Table 6. Kinetic parameters for sorption of Pb(II) onto ZnAl mixed oxide/PVA nanocomposite at different temperatures.

T, K	Pseudo-first-order			
	k_1	$q_{e,\ calc.}$	$q_{e,\ exp.}$	r^2
298	0.049	19.3	245.3	0.884
313	0.008	911	1599	0.859
333	0.024	1.63	161.2	0.919
	Pseudo-second-order			
298	k_2	$q_{e.hes.}$	$q_{e,\ təc.}$	R^2
313	0.00048	250	245	0.993
333	0.000031	1562	1599	0.950
	Weber and Morris			
298	k_{WM}	C	R^2	k_{WM}
313	-4.544	270.8	0.740	-4.544
333	70.54	581.6	0.785	70.54

The adsorption capacity value of ZnAl mixed oxide/PVA nanocomposite for Pb^{2+} ions sorption described in this work is much higher than other previous works. Thus, ZnAl mixed oxide/PVA nanocomposite is an efficient adsorbent for the sorption of Pb^{2+} ions.

Removal of Tartrazine, Ponceau 4R (P4R) and Patent blue –V (PB-V) synthetic food dyes from aqueous solutions by ZnAl-LDH / PVA nanocomposite. The analysis of ZnAl-LDH/PVA nanocomposite by X-ray diffractometer shoü that, the splitting of the peak is at $2\Theta = 12.02^o$ and 12.62^o angles clearly visible. Here the main reason for splitting is the formation of tense (sharp peak) and relaxation (broad peak) phases due to the long crystallization time. After the sorption of dyes composites were separated from the solution, dried and XRD analysis was performed. At 2 and 9 pH values, the splitting of the diffraction peaks disappeared, and one sharp peak (strained phase) was observed at all diffraction angles. The disappearance of the broad peak in strongly acidic (pH = 2) and alkaline (pH = 9) environments is explained by the presence of only the tense phase in the aggressive environment.

The average particles size increases after the sorption of dyes, which indicates that the intercalation is going in the LDHs. With the sorption of tartrazine, P4R, and PB-V, the basal distance of ZnAl-LDH increased from 7.008 Å to 7.490 Å, 7.250 Å, and 7.110 Å, respectively.

However, the splitting of the diffraction peaks increased with the sorption of PB-V. At this time, intercalation of the zwitter ion with the anion field and interlayer distance widened, as the cation field had a repulsive interaction with the "+" charged layers, the layers underwent a high expansion.

The IR spectra of nanocomposites obtained before and after the sorption are given in **Figure 22**. Since the formation of the constructed polymer occurred at the same time as the formation of ZnAl-LDHs, the layers of the LDHs were compacted and water molecules left the interlayer distance. The formation of a wide absorption band at those frequencies in the spectra of the nanocomposite is explained by the intercalation of LDHs due to the sorption of dyes.

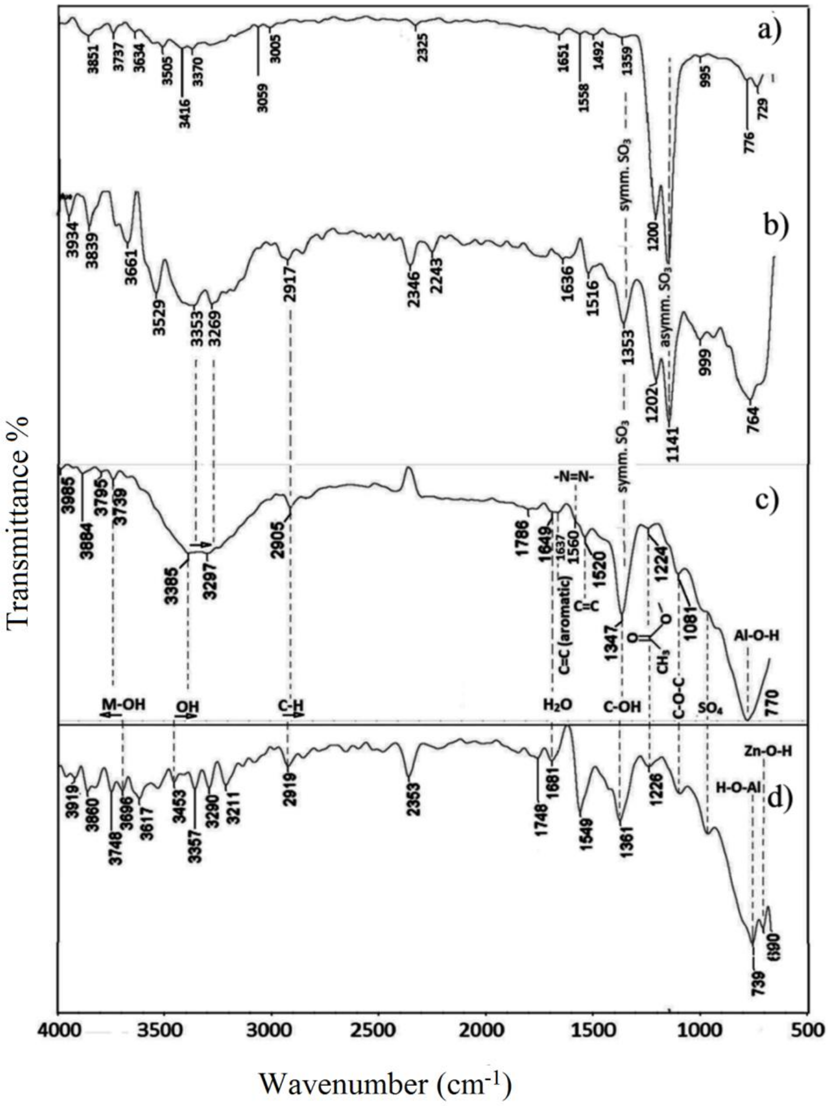

Figure 29. IR spectra of a) P4R, b) PB-V, c) tartrazine sorbed, and d) pure ZnAl-LDH/PVA nanocomposite.

In the PB-V molecule, the sulfo groups are located close to each other, so they are directed to only one layer of the LDH, and only one sulfo group in each molecule interacts with the positively charged layer of the LDH, while the other is free and appears with a clear intensity in the IR spectrum. However, since the sulfo groups in tartrazine are located far from each other, this distance corresponds to the interlayer distance in LDH, and the sulfo groups in the molecule are directed towards the opposite layers of LDH and participate in the interaction with the positively charged layers of LDH by the sorption of tartrazine. Knowing that the symmetric and asymmetric valence oscillations corresponding to the SO_3- group in alkyl and aryl sulfonates belong to the frequencies of 1369-1290 cm^{-1} and 1170-1120 cm^{-1}, since there are 3 aryl sulfonate groups in one P4R molecule, the sorption band corresponding to this group was observed with high intensity.

The maximum adsorption (~95%) occurred at the initial concentrations of tartrazine, P4R and PB-V on 25, 15 and 6 mg/l, respectively. The Temkin isotherm model is the most suitable model for the adsorption of taken dyes onto ZnAl-LDH/PVA nanocomposite. Also, the adsorption of Tartrazine suitable the Langmuir model, and the sorption of P4R and PB-V follows the Freundlich model. The fit of sorption to both Langmuir and Freundlich models indicates that adsorption centers are both homogeneous and heterogeneous. This may be due to the complex composition of the nanocomposite.

Based on the values of activation energies calculated for tartrazine (E = 0.941kC/mol), P4R (E = 0.78) and PB-V (E = 1.52), it is possible to say that in these systems, sorption is physical in nature.

In order to determine the interparticle diffusion, graphs of the equilibrium values of sorption capacity (STtar.) at different temperatures (293 K, 303 K and 313 K) versus the sorption time were constructed and shown in **Figure 23**.

Each plot is divided into two or three linear sections, of which the first, second, and third sections are treated as surface or boundary layer diffusion, intraparticle or pore diffusion, and equilibrium diffusion, respectively. As can be seen, the optimum temperature for the adsorption of tartrazine on ZnAL-LDH / PVA nanocomposite was 303 K and the maximum sorption degree (R %) was determined to be 96.2 % at 50 min.

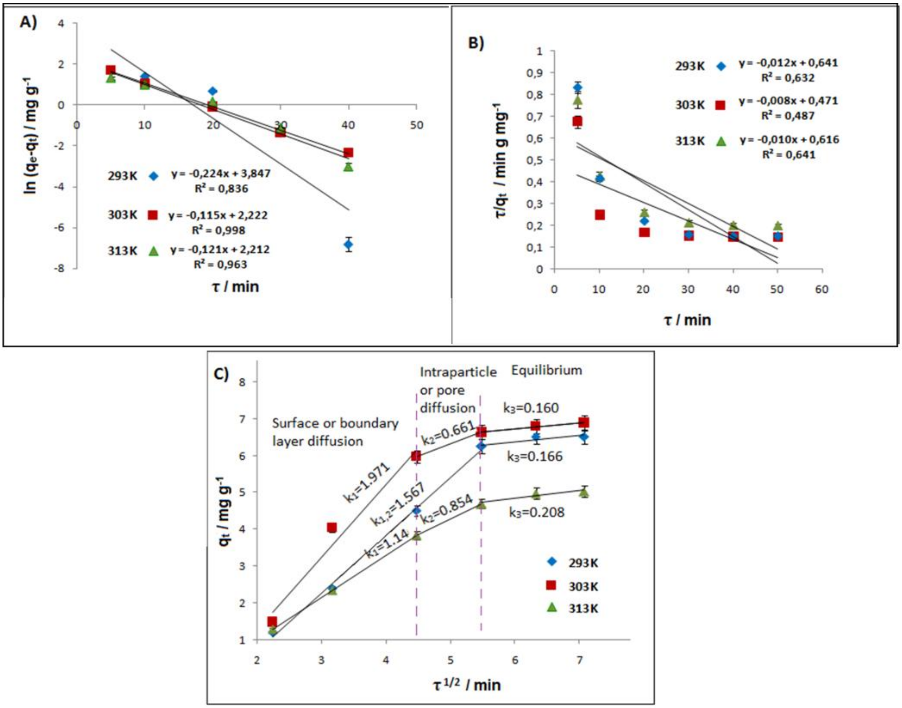

Figure 23. Kinetic models for the adsorption of tartrazine on ZnAl-LDH/PVA nanocomposite.

In Chapter VII, the application of obtained nanocomposites to photocatalysis and their regularities are discussed.

It was determined that the synthesized ZnAl-LDH/PVA nanocomposite is a very good photocatalyst for tartrazine and P4R dyes under ultraviolet and visible light. Adsorbent reuse was achieved by photodegradation of adsorbed dye molecules on the nanocomposite. The increase of the d_{003} diffraction parameter after cyclic use caused more tartrazine anions to enter the interlayer space in each subsequent sorption process, and the use of the nanocomposite could be repeated many times. The probable mechanism of photodegradation of tartrazine in ZnAl-LDH/PVA nanocomposite is given in **Figure 24:**

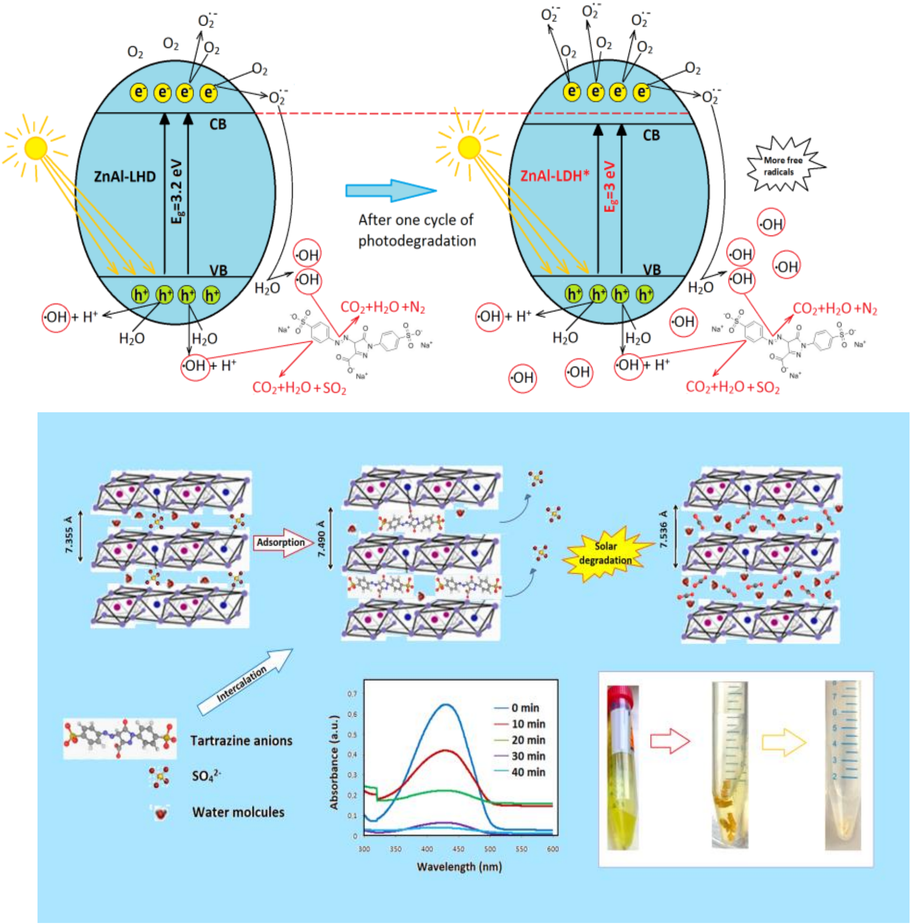

Figure 24. Schematic representation of the photocatalytic decomposition of tartrazine on ZnAlLDH/PVA nanocomposite.

The layers of the nanocomposite intercalated with tartrazine anions moved away from each other to a certain extent, and during degradation, the layers did not become denser, on the contrary, they expanded a little more (d003 = 7.358 → 7.490 → 7.536 Å). An increase in the d003 parameter after repeated use caused more

Tartrazine anions to enter the interlayer space in each subsequent sorption process, increasing the reusability of the nanocomposite.

Photocatalytic degradation of Ponceau 4R (E124) food dye by ZnAl-LDH synthesized in the presence of PVA and without polymer. Zinc oxide (ZnO) and zinc hydroxides (λ,α,β) $Zn(OH)_2$ were obtained along with during the formation of ZnAl-LDH/ PVA nanocomposite. The main reason for this is the different crystallization rates of nanocrystals and the high concentration of the alkaline solution. Thus, ε-$Zn(OH)_2$ (ICSD # 50447) with orthorhombic structure and space group P212121, α- $Zn(OH)_2$ (JCPDS No. 41–1359) with tetragonal lattice parameters a = b = 6.825 and c = 33.36 and β-$Zn(OH)_2$ (JCPDS No. 24–1444) with hexagonal lattice parameters a = b = 3.192 and c = 4.65 was crystallized (**Figure 25**). The splitting of diffraction peaks disappeared after the sorption, partially returned to previous state after the photodegradation, and basal space became wider. The splitting of the diffraction peaks disappeared after sorption. After the P4R-sorbed nanocomposite was irradiated under sunlight without separating from its aqueous solution, the diffraction pattern of the nanocomposite partially returned to its previous state due to the decomposition and mineralization of the dye, and at the same time, the basal cavity was further expanded. In this case, the peak falling on the (003) Miller index plane shifted to a lower diffraction angle, and the peak splitting occurred again. Although the intercalation is not so high (7.00 Å > 7.62 Å), the gap width of ZnAl-LH(ACTB) and ZnAl-LH/PVA samples is from 3.23 eV to 2.87 eV and decreased significantly from 3.25 eV to 2.82 eV. Such a sharp reduction in the width of the forbidden zone increases the reusability of the catalyst. Thus, the activity of a catalyst used once in photodegradation increased with each subsequent use. The energy required for electron transfer from the 2p level of oxygen to the conduction level of Zn and Al is reduced. Although the average particle size decreased with the increase of the basal distance, the stability of the layers also weakened as the physical forces between the layers weakened.

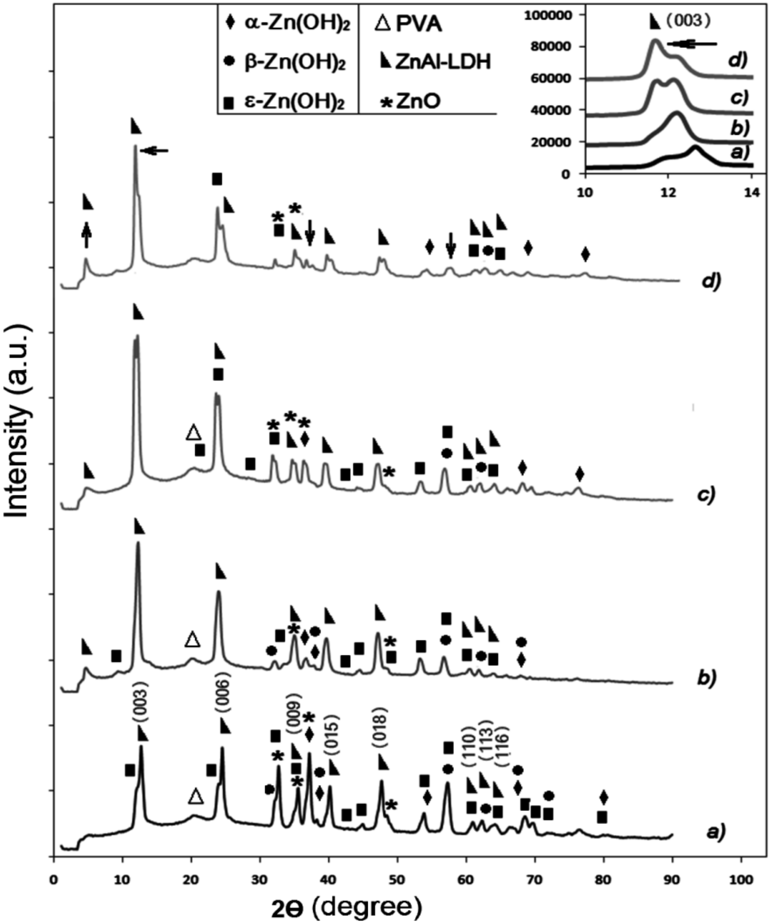

Figure 32. XRD patterns of ZnAl LDH/PVA nanocomposite: a) initial, b) after sorption of P4R, c) in intermediate photodegradation state of P4R, and d) after complete photodegradation of P4R.

After the photodegradation of P4R, the bandgap of the nanocomposite decreased, and the transition energy of the electron from the 2p level of oxygen to the conducting level of Zn and Al increased.

The PL analysis of PVA and Zn-Al LDH/PVA nanocomposites are show that, polymer-related emissions were observed in both spectra. Due to increased surface defects and sufficient surface wear, higher emission corresponding to ZnAl-LDH was observed due to molecular interaction. Deep-level emission (DSE) appears in the spectrum of the nanocomposite. The more intense maximum indicates the recombination of free excitons, while the other produces deep-level defects such as O-vacancy and Zn-interstitial[12].

The effect of pH on photocatalyst activity was also studied. The surface of ZnAl-LDH will be positively charged in acidic environment and negatively charged in alkaline environment. Since ZnAl-LDH itself consists of positively charged layers, the concentration of positive charges will increase in an acidic environment. This is a good situation for the adsorption of anionic dyes. As the number of OH- particles increases in the alkaline medium, the surface of the ZnAl-LDH catalyst will become neutral. In this case, physical adsorption will prevail and absorption will occur only in the pores of the nanocomposite. In acidic and alkaline environments, the nanocomposite will have the following form:

$$Zn_3Al[(OH)_6]^{+3} \cdot 3(NO_3^-) \cdot 9H_2O + nH^+ \rightarrow$$

$$\rightarrow Zn_3Al[(OH)_6]^{+3} \cdot nH^+ \cdot 3(NO_3^-) \cdot 9H_2O$$

$$Zn_3Al[(OH)_6]^{+3} \cdot 3(NO_3^-) \cdot 9H_2O + nOH^- \rightarrow$$

$$\rightarrow Zn_3Al[(OH)_6]^{+3} \cdot nOH^- \cdot 3(NO_3^-) \cdot 9H_2O$$

ZnAl-LDH was taken as a catalyst in the study and the sorption rate was maximum at pH = 2 and 4. Since photodegradation is caused by the destructive effect of ·OH radicals on dye molecules, the increase of OH- ions can also play an important role[13,14]. Because OH- combines the hole (h +) particle to form the ·OH radical.

---

[12] Zhang, Z. Eco-friendly nanostructured Zn-Al layered double hydroxide photocatalysts with enhanced photocatalytic activity / Z. Zhang, Z. Hua, J. Lang [et al.] // CrystEngComm, - 2019. 21, - p. 4607–4619.

[13] Bouarroudj, T. Photodegradation of tartrazine dye favored by natural sunlight on pure and (Ce, Ag) co–doped ZnO catalysts / T. Bouarroudj, L. Aoudjit, L. Djahida [et al.] // Water Science and Technology, - 2021. 83, - p. 2118. doi:10.2166/wst.2021.106

$$OH^- + h+ \rightarrow OH\cdot$$

However, the complete decomposition of the dye molecules in the photocatalyst and the regeneration of the catalyst was 100% within 5 h at pH-7.

The rate of photocatalytic decomposition of P4R on ZnAl-LDH/PVA nanocomposite and ZnAl-LDH was studied by Langmuir–Hinshelwood (L-H) kinetic model.

The Langmuir constant (K_L = 0.102) of P4R dye adsorption on ZnAl-LDH / PVA nanocomposite is close to the Langmuir – Hinshelwood constant ($K_{L\text{-}H}$ = 0.094). However, the values of these two constants in the ZnAl-LDH catalyst synthesized without the presence of PVA differ sharply (K_L = 0.021, $K_{L\text{-}H}$ = 0.001). We know that the value of K_L is inversely proportional to ST_{max} and k_c, and since K_L is explained by the Gibbs free energy between sorbent and sorbate molecules, a high value of K_L indicates a strong interaction between sorbent and sorbate molecules. Due to the high ability of LDHs to capture the dye molecule, sorption and photodegradation are provided in right direction.

According to the plot of $\ln(C_0/C)$ as a function of irradiation time, the rate constants of photodegradation of P4R onto ZnAl-LDH/PVA nanocomposite increased from 0.0232 to 0.026, and decreased from 0.026 to 0.0177 when the concentration reached to 30 mg/l and 50 mg/l, respectively.

The photodegradation of P4R dye proceeded as follows:

$$C_{20}H_{11}N_2Na_3O_{10}S_3 + Zn_3Al[(OH)_6]^{+3}(NO_3^{-)} \cdot 9H_2O \rightarrow$$

$$\rightarrow Zn_3Al[(OH)_6]^{+3} \cdot x\ C_{20}H_{11}N_2O_{10}S_3{}^{3-} \cdot 9H_2O$$

$$\text{ZnAl-LDH (with and without PVA)}+h\nu \rightarrow \text{ZnAl-LDH } (e^- + h^+)$$

$$H_2O + h^+ \rightarrow \cdot OH + H^+$$

$$2H_2O + 2h^+ \rightarrow H_2O_2 + 2H^+$$

---

[14] Chen, Y. Role of primary active species and TiO2 surface characteristic in UV-illuminated photodegradation of Acid Orange 7 / Y. Chen, S. Yang, K. Wang [et al.] // Journal of Photochemistry and Photobiology A: Chemistry, - 2005. 172, - p. 47–54. https://doi.org/10.1016/j.jphotochem.2004.11.006

$H_2O_2 + h\nu \rightarrow 2\ {}^{\cdot}OH$
$h^{+} + OH^{-} \rightarrow {}^{\cdot}OH$
$O_2 + e^{-} \rightarrow O_2^{\cdot -}$
$H_2O + O_2^{\cdot -} \rightarrow H_2O_2$
$O_2^{\cdot -} + H_2O_2 \rightarrow {\cdot}OH + OH^{-} + O_2$
$P4R_{ads} + h\nu \rightarrow P4R^{*}_{ads}$
$P4R^{*}_{ads} \rightarrow P4R^{\cdot +}_{ads} + e^{-}$
$P4R + e^{-} \rightarrow P4R^{\cdot -}$
$P4R + h^{+} \rightarrow P4R^{\cdot +}$
$Zn_3Al[(OH)_6]^{+3} \cdot x\ C_{20}H_{11}N_2O_{10}S_3^{\ 3-} \cdot 9H_2O + {}^{\cdot}OH \rightarrow$
Photodegradation products + $Zn_3Al[(OH)_6]^{+3}(NO_3^{-}) \cdot 9H_2O$ (regenerated catalyst)

The specific surface area of the noncomposite was 4.9 m^2 /g and 11.65 m^2 /g by BET analysis before and after photodegradation of P4R, respectively. An increase in the specific surface area means an increase in the photocatalytic activity of the catalyst.

In the nanocomposite obtained without the presence of PVA, the rate constant (k) of photodegradation decreased from 0.044 to 0.0437 at low concentrations of the pollutant in the aqueous solution and increased from 0.0437 to 0.0481 with the subsequent increase the initial concentration of the dye. Such a contrasting change in reaction rate constants in nanocomposites obtained with and without PVA can be explained by various factors. At this time, the approach of dye molecules to the active surface of the ZnAl-LDH nanocomposite catalyst is limited by the low amount of the dye solution. As the concentration of the solution increased, this probability also increased to a certain extent.

In the ZnAl-LDH / PVA nanocomposite, the dye molecules first enter the nanopores of the polymer nanocomposite in a low-density dye solution. In this case, the surface of the photocatalyst is activated by light, which easily interacts with the dye molecules. PVA captures the dye molecules and transfers them to the surface of the ZnAl-LDH ionic conductor. In the absence of PVA, the probability of low concentration dye molecules approaching the catalyst surface is reduced. With increasing concentration of dye molecules, the rate constant of photodegradation on ZnAl-LDH nanocomposite obtained by using PVA decreased (from 0.025 to 0.0177) and increased without PVA (from 0.043 to 0.048). Such cases are also directly related to the polymer matrix. As the polymer covers the surface of the LDH, it carries a certain number of dye molecules to the surface. However, the large size of the dye molecules and the increase in their concentration in the solution reduce their sorption rate in the polymer.

Polar gas molecules formed as a result of rapid decomposition of Ponso 4R molecules separated from the catalyst surface, and the rapid movement of gas molecules under light increased the chaotic movement of heavy dye molecules. Thus, the capture of the catalyst surface was prevented and the photodegradation was accelerated. The acceleration of decomposition is also explained by the fact that the released polar gas molecules absorbed light and emitted it to a nearby catalyst.

After photocatalytic decomposition, water was separated from the nanocomposite and the amount of Zn^{2+} and Al^{3+} ions in the solution was analyzed by ICP. The concentrations of Zn^{2+} and Al^{3+} ions returning from the sorbent to the solution were 14.906 mg/l and 0.040 mg/l, respectively. However, the return of Al^{3+}-ions to the solution is significantly less, and the amount of Zn^{2+} ions in drinking water (exceeds the maximum allowed amount (5 ppm) of the World Health Organization (WHO) and the Environmental Protection Agency). The amount of Zn^{2+} has decreased to 4.105 mg/ l with periodic use of the catalyst.

Photodegradation of Ponceu 4R and Rhodamine 6G (R6G) dyes by alkaline earth, transition and rare earth metal-doped ZnAl-LDH/PVA nanocomposites.

As can be seen from **Table 7**, the sorption rate of pure nanocomposite (50.98 %) increased with Cd, Cu, Fe, Co, Ni and Ca doped elements, and decreased with Ag and Sr. The maximum adsorption rate was observed with Cu and Cd metals in the anionic dye due to the increase of positive charges. In contrast to adsorption, the photodegradation rate of undoped ZnAl-LDH/PVA nanocomposite with anionic dye (P4R) is high (92.07%), but this result is enhanced by Cd, Fe, Ag, Co, Sr and Ca elements. Bandgap decreased from 3.12eV to 3.1eV with Sr and Ag, 3.09eV with Pb, 3.08eV with Cd, 3.06eV with Co, 3eV with Cu and Ni, 2.6eV with Fe and 2.2eV with La dopants.

Table 7. Sorption and photodegradation of P4R anionic dye on pure and doped ZnAl-LDH/PVA nanocomposite.

Doped metals	-	Cd	Cu	Fe	Ag	Co	Ni	Sr	Ca	Pb
SD %	51,98	64,40	66,54	54,92	43,47	54,74	55,99	45,97	51,87	41,68
PD %	92,07	94,09	60,08	94,90	93,10	93,48	89,00	95,32	92,26	91,04

As can be seen from Table 8, ZnAl-LDH/PVA nanocomposite is an excellent photocatalyst for cation-type dye (R6G). The efficiency from adsorption to photodegradation increased from 19.59% to 88.54%

Table 8. Sorption and photodegradation of R6G cation-type dye on pure and doped ZnAl-LDH/PVA nanocomposite.

Aşqar metal	-	Cd	Cu	Fe	Ag	La	Ni	Sr	Ca	Pb
SD %	19,59	23,51	16,45	10,68	19,00	5,78	10,97	17,43	16,93	10,58
PD %	88,54	79,43	66,01	57,98	81,78	67,9	66,11	81,3	75,51	65,13

Photodegradation of methylene blue and congo red dyes by C_{60}-***doped ZnAl-LDH/PVA* nanocomposite.** The sorption and photocatalytic properties of the synthesized and C_{60}-doped ZnAl-LDH/PVA nanocomposites were studied on methylene blue (MB) and Congo red (CR) cationic and anionic organic pollutants. Photodegradation of dyes from aqueous solutions was carried out under 150 W light at room temperature in the presence of a permanent magnetic stirrer. The distance between the sample and the light was taken as 10 cm. Discoloration of solutions were measured y using UV-Vis spectrometer keeping an interval of 1 hour between them, and the photodegradation degree of nanocomposites was calculated. Since LDHs consist of positively charged layers, they are very good sorbents for the sorption of anions. Therefore, the sorption capacity and degree of CR in the synthesized nanocomposites is higher than that of MB. Doping of C_{60} was performed to increase the sorption rate of cationic dyes in anionites.

The sorption of CR in C_{60}-added and pure LDH mainly conformed to the Langmuir model, and the sorption increased due to electrostatic forces. In contrast, the sorption rate of MB on pure LDH increased dramatically (from 3.2% to 50%) from 5 mg/L to 25 mg/L concentration of dye molecules. This can be caused by electrostatic mutual repulsion: when the concentration of dye molecules is low in the solution, their repulsion from the surface of the sorbent is strong. Since C_{60} has a negative zetta potential (-88 mV), their incorporation into LDHs increases the sorption of cationic dye molecules. The sorption rate of C_{60}-doped LDH increased from 42% to 59% by increasing the initial concentration of MB from 5 mg/L to 25 mg/L (**Table 9**).

Table 9. Photodegradation parameters of dyes onto C_{60} doped ZnAl-LDH/PVA nanocomposite in 360 minutes.

Samples	SD (%)	PD (%)	k_{app} (min^{-1})	R^2
For MB				
ZnAl-LDH/PVA	48.46	81.63	0.002	0.986
10%C_{60}/ZnAl-LDH/PVA	57.24	89.16	0.003	0.970
20%C_{60}/ZnAl-LDH/PVA	85.55	96.98	0.004	0.890
60%C_{60}/ZnAl-LDH/PVA	59.76	87.47	0.003	0.976
For CR				
ZnAl-LDH/PVA	68.00	91.37	0.017	0.940
1% C_{60}/ZnAl-LDH/PVA	95.3	98.78	0.024	0.802

In this case, the optimal amount of C_{60} for ZnAl-LDH/PVA nanocomposite is 20%.

To determine the active species like hydroxyl radical (•OH), superoxide anion radical (•O_2-) and holes (h+) involved in photodegradation. A significant decrease in the photodegradation rate of MB and CR in the presence of ascorbic acid and IPA proves that the photodegradation goes in the presence of $\bullet O_2$- anion radicals and •OH radicals, respectively (**Figure 26**). In previous works [15], it was determined that the effect of active species is the same or very similar for different dyes (MB and CR) on the same catalyst. The research shows that although all known active species are formed on the surface of the catalyst and in the environment, the nature of the dye molecules also affects which active species is responsible for photodegradation.

The probable mechanism of photodegradation of MB and CR dyes onto C_{60}/ZnAl-LDH/PVA nanocomposite is given in **Figure 27**.

As can be seen, after addition of C_{60}, the bandgap of the nanocomposite decreased and the Urbach zone was formed. As a result of irradiation, the electrons in the p level of carbon covered the valence band and due to the resulting Urbach band, the transition energy of electrons to the conduction band decreased.

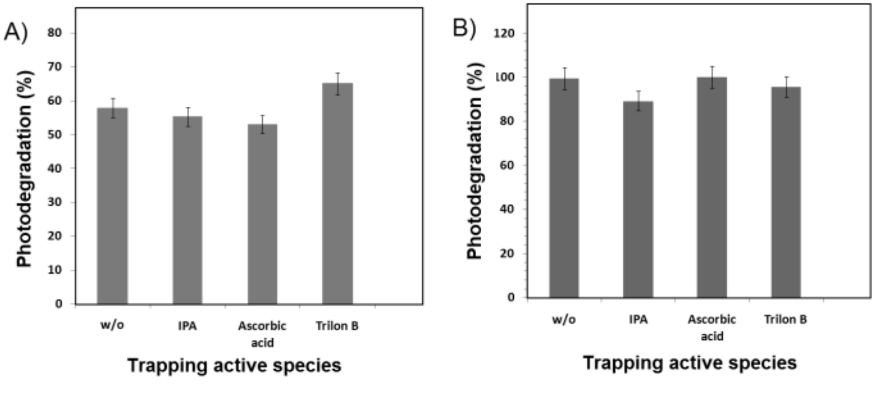

Figure 26. Active spaces trapping of Methylene blue (A) and Congo red (B).

---

[15] [1]Saleh, R. A. Degradation of Methylene Blue and Congo-Red Dyes Using Fenton, Photo-Fenton, Sono-Fenton, and Sonophoto-Fenton Methods in the Presence of Iron(II,III) Oxide/Zinc Oxide/Graphene (Fe_3O_4/ZnO/Graphene) Composites / Saleh, R.; Taufik, A. // Sep. Purif. Technol. -2019. 210, -p. 563–573.

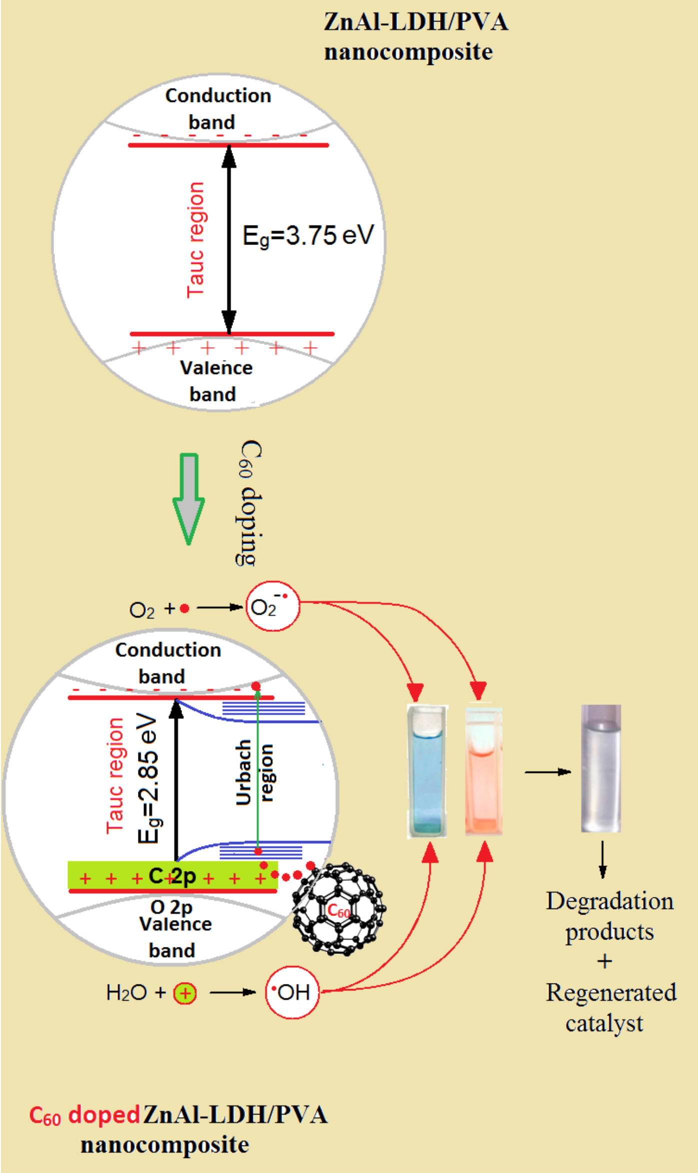

Figure 38. Probable mechanism of photodegradation of MB and CR dyes onto C_{60}/ZnAl-LDH/PVA nanocomposite.

RESULTS

1. CoCr, CoAl, ZnAl, NiZnAl, CdZnAl layered double hydroxides, ZnO and $Zn_6Al_2O_9$ metal oxides, $Ni_xZn_{1-x}S$, $Cd_xZn_{1-x}S$ və $Cu_xCd_{1-x}S$ ternary sulfides with PVA and functionalized nitrile rubber were synthesized and doping of obtained LDHs with the alkali-earth- (Ca, Sr), transition- (Co, Cu, Cd, Ni, Pb, Fe), noble- (Ag), rare earth- (La) elements and fullerene was carried out, and the sorption and photodegradation of dyes and metal ions were studied in this work. It was possible to influence the properties, size, bandgap, morphology, sorption and photocatalytic properties of nanoparticles by changing the reaction parameters, the order of processing of reagents, the proportion of metals, intercalating agents, the nature of anions and the percentage of polymer in nnomaterials [1-63].

2. Synthesis and modification of CoCr-LDH and monohydroxides show that, α- and β $Co(OH)_2$ along with LDH and amorphous $Cr(OH)_3$ were formed at low pH values (pH~7) and in excess amount of Cr, respectively. The basal space of CoCr-LDH increased from 7.366 Å to 7.428 Å and 25.214 Å, after the intercallation with ST and NaSt, respectively and the reaction resulted in high crystallization at high concentrations of the alkaline solution. The reduction of the average particle size after the intercalation, is due to the enter of organic groups into the interlayer space and fragmentation of the particles [3,4,6-10,12].

3. ZnAl-LDHs and ZnO nanoparticles were formed in respective <2M and >2M concentrations of NaOH. According to X-ray diffraction results of ZnAl-LDH nanoparticles synthesized with 2M and 5M NaOH, formation of characteristic peaks of ZnO phase along with hydrotalcite structure was explained by the amphoteric property of Al. Carbonate anions released when urea was used in the synthesis were intercalated into the layers of LDHs and the basal space was determined as 9.51Å.

4. The diffraction peak of PVA shifted to upper angle with the formation of ZnAl-LDH /PVA nanocomposite by co-formation method and cross-linking of PVA has taken place by means of LDHs. The reason for the smaller average particle size in ZnAl-

mixed oxide/PVA nanocomposite, that PVA covers the LDH particles and prevents further growth of nanoparticles [39,40,42].

5. SEM observation of flower and star-shaped morphology of ZnAl-mixed oxide/PVA nanocomposite proves that two types of crystals (ZnO and $Zn_6Al_2O_9$) are formed and indicates the formation of a strong -Zn-O- bond, in which each of the particles is composed of rod- and needle-shaped nanocrystals. For ZnO and $Zn_6Al_2O_9$ nanocrystals contained in the nanocomposite, two types of optical electronic transition related to the Zn-O bond were determined: between the 1) filled 2p orbitals of oxygen and 4p and 4s orbitals of zinc; 2) filled 2p orbitals of oxygen and the empty 3s orbitals of aluminum in the $Zn_6Al_2O_9$ crystal [22,33].

6. The mechanism of sorption was mainly based on the pseudo-second-order kinetic model and the Freundlich isotherm. After nine cycles of reuse, the sorption rate of Pb^{2+} ions was 63.177%. This result indicates that the regeneration of the sorbent is high [14,15,18].

7. The shift of the specific diffraction peaks of ZnAl-LDH towards lower diffraction angles and the increase in the average size of nanocrys-tallites after sorption of tartrazine, P4R and PB-V dyes in ZnAl-LDH/ PVA nanocomposite obtained by co-formation is explained by the inter-calation of dye molecules into the layers of LDH. Regeneration of nanocomposite was ensured by photo-degradation and performance of sorption and photodegradation increased by reuse [23,25,31,32,34,35,52].

8. The photodegradation of P4R on ZnAl-LDH and ZnAl-LDH/PVA nanocomposites was studied under sunlight. In the ZnAl-LDH/PVA nanocomposite, all the diffraction peaks corresponding to the LDH are split with the formation of relaxed (broad) and strained (sharp) phases. The relaxed phase was lost by the intercalation of the dye molecules into the LDH, but was restored by photodegradation. [31,32,34,35,52].

9. Although the intercalation is not high (7.00 Å-> 7.62Å), the band-gap is reduced, the reusability and efficiency of the catalyst has increased in ZnAl-LDH and ZnAl-LDH/PVA after the photodegradation of P4R. The value of the Langmuir constant (K_L = 0.102) was close to the value of the Langmuir-Hinshel-wood

constant (K_{L-H} = 0.094) obtained from kinetic calculations, and sorption and photodegradation were ensured in the right direction [31,32,34,35,52].

10. Effective sorption and photodegradation of PB-V from aqueous solutions of ZnAl-LDH/PVA nanocomposite showed that the reusability of the sorbent is related to the structure and optical properties of the nanocomposite. The optimal sorption of the nanocomposite at both low and high pH was explained by the fact that the PA-V dye molecule is a zwitterion.Partial changes in structural parameters, basal spacing, particle size, and bandgap by sorption and photodegradation were explained by intercalation into PB-V in ZnAl-LDH/PVA nanocomposite [34,49,55].

11. $Cd_xZn_{1-x}S$ nanoparticles were synthesized by direct sulfidation of CdZnAl-LDH/PVA nanocomposite and the obtained nanocomposites were applied to photodegradation of m-cresol from water. The significant increase of photocatalytic activity of CdZnAl-LDH/PVA nanocomposite after the sulfidation is related to the reduction of particle size, increase of surface area, complete sulfidation, and dispersed distribution. The photodegradation was accelerated by increasing the radicals amount [45,53,54,59,61].

12. $Cd_xZn_{1-x}S$ nanoparticles were synthesized by SILAR method on the base of FNBR. The effect of Cd:Zn on the optical, paramagnetic, structural, dielectric, thermal properties and surface morphology was studied in detail. The stability of the ternary sulfide increased with increasing cadmium content in crystal lattice. The average size of nanoparticles is ~25-50 nm by SEM and ~10-20 nm by TEM. EPR spectra of CdS/FNBR nanocomposite are broad, singlet asymmetric and have isotropic symmetry ($g_x=g_y=g_z$). Compared to NBR, FNBR has shown significant thermal stability, and its application as a stabilizer in the formation of nanoparticles is very favorable [2,5,16,20,24,36,37,62].

13. $CdCuS_2$ nanoparticles were synthesized by the SILAR method based on FNK, in 3 periods, peaks corresponding to CdS and 15 periods corresponding to CuS prevailed, and the crystal lattice of binary sulfides became dominant in the corresponding periods, which is explained by the effect of supersaturation and chemical potential.

The wide band gap (~3.7 eV) obtained for CuCdS2/FNK is due to the fact that the formation of nanoparticles takes place in the limited volume of FNK [11,29,50,51,63].

14. ZnAl-LDH/PVA nanocomposite non-covalently doped with fullerene. The average size of the obtained nanocrystallites increased, and the dislocation density (δ) decreased from. The X-ray diffraction peaks of the fullerene-doped nanocomposite were observed at lower angles, the basal distance increased. Complete photodegradation of MB in the nanocomposite occurred with 10 h of illumination (~99%). With a high amount of fullerene, the active centers on the surface of ZnAl-LDH were covered, and as a result, the ionic conductivity of ZnAl-LDH was reduced. It was found that as a result of photocatalytic oxidation, all known active species are formed on the surface of the catalyst, but the nature of the dye molecules affects photodegradation mainly occurs at the expense of which active species [56-58].

15. In order to increase the sorption and photodegradation capacity of the obtained nanocomposites, ZnAl-LDH/PVA is doped with alkaline-earth (Ca, Sr), transition- (Co, Cu, Cd, Ni, Pb, Fe), noble-(Ag) and rare earth- (La) elements by impregnation method. In contrast to the anionic dye, the cationic dye could not enter the layers of LDH, so the sorption occurred on the surface. The maximum sorption rate was observed with Cu and Cd dopant metals in the anionic due to the increase of positive charges. The bandgap is decreased after the doping of ZnAl-LDH with Sr, Ag, Pb(II), Cd, Co(III), Cu(II), Ni(II), Fe(II) and La(III) elements, respectively. It was found that the nature of doping elements has a direct effect on the recombination of h+ and e- pairs and the decomposition of dyes by generating radicals [19,21,26,27,28,30,38,40,41,46].

Scientific works published on the subject of the dissertation:

1. Muradov, M.B. Synthesis and characterization of cobalt sulfide nanoparticles by sonochemical method / M.B.Muradov, O.O.Balayeva, A.A.Azizov [et al.] // Infrared Physics & Technology, -2018. 89, -p. 255-262. **Web of Science.**

2. Maharramov, A.M. Effect of metal ions on the thermal degradation of chlorophosphorylated NBR / A.M.Maharramov, A.A.Azizov, O.O.Balayeva [et al.] // New Materials, Compounds and Applications, -2018. 2, -p. 5-9. **Web of Science.**

3. Balayeva, O.O. Synthesis, Modification and Optical Characterization of Co-Cr Layered Double Hydroxide / O.O.Balayeva, A.A. Azizov, M.B. Muradov [et al.] // Journal of Materials and Applications, -2018. 7 (2), –p. 90–95.

4. Balayeva, O.O. Synthesis and optical characterization of cocr–ldhs using different concentrated base solutions (C_{NaOH}= 10M and 20M) / A.A. Azizov, M.B. Muradov, G.M.Eyvazova // Journal of Baku Engineering University, Baku: –2018. 2 (2), –p. 102-106.

5. Balayeva, O.O., Əzizov, A.Ə., Muradov, M.B., Alosmanov, R.M. $Cd_xZn_{1-x}S$ üçlü metal sulfid nanoquruluşlarının sintezi və tədqiqi // Akademik Murtuza Nağıyevin anadan olmasının 110 illiyinə həsr edilmiş beynəlxalq konfrans, -Bakı: - 27-28 October, –2018. –s. 206.

6. Balayeva, O.O. Əzizov, A.Ə., Muradov, M.B. Synthesis of Co(II)Cr(III)-layered double hydroxide and nitrile butadiene rubber based nanocomposites // II International scientific conference of young researchers. Baku Engineering University, -Baku: -27-28 April, –2018. –p. 198-200.

7. Balayeva, O.O., Əzizov, A.Ə., Muradov, M.B., Maharramov, A.M. Co(II)Cr(III)-LDH/NBR nanocomposites: synthesis and optical characterization // Magistrların və gənc tədqiqatçıların «Fizika və astronomiya problemləri» Beynəlxalq elmi konfransı, -Bakı: -24-25 May, –2018. –p. 246-249.

8. Balayeva, O.O., Əzizov, A.Ə., Muradov, M.B., Maharramov, A.M. CoIICrIII – əsaslı laylı ikili hidroksidlərin müxtəlif temperaturlarda sintezi // Ümummilli Lider Heydər Əliyevin anadan olmasının 95-ci ildönümünə həsr olunmuş XII Respublika Elmi Konfransı «Kimyanın aktual problemləri» , -Bakı: -25-26 May, –2018. –s. 170-171.

9. Balayeva, O.O. Cobalt chromium-layered double hydroxide, α- and β- $Co(OH)_2$ and amorphous $Cr(OH)_{3:}$ synthesis, modification

and characterization/O.O.Balayeva, A.A.Azizov, M.B.Muradov, R.M. Alosmanov // Heliyon, –2019. 5, –p. 1-7. **Web of Science.**

10. Balayeva, O.O. CoCr-laylı ikili hidroksidlərin sintezinə müxtəlif reaksiya parametrlərinin təsiri / O.O.Balayeva, Azizov A.A., Muradov M.B // Bakı Universitetinin Xəbərləri. Təbiət elmləri seriyası, –2019. №1, –s. 31-38.

11. Gahramanli, L.R. The influence of temperature and concentration of solutions to physical properties of Cu_xS nanoparticles / L.R.Gahramanli, M.B.Muradov, O.O.Balayeva, G Eyvazova, [et al.] // Chalcogenide Letters –2019. 16, –p. 587-594. **Web of Science.**

12. Balayeva, O.O., Əzizov, A.Ə., Muradov, M.B., Eyvazova, G.M. Kobalt-xrom əsaslı laylı ikli və qarışıq hidroksidlərin sintezi // III International scientific conference of young researchers. Baku Engineering University, -Baku: -22-23 April, – 2019. –p. 541-543.

13. Balayeva, O.O., Əzizov, A.Ə. Dövri sistem tədrisdə // Kimyanın aktual problemləri". Ümummilli Lider Heydər Əliyevin anadan olmasının 96-ci ildönümünə həsr olunmuş XIII Beynəlxalq Elmi Konfrans, -Bakı: -15-16 May, 2019. –p. 15-17. .

14. Balayeva, O.O., Mürsəlova, G.Q., Rəhimli, K.S., Əzizov, A.Ə. Zn-Al əsaslı LİH-lərin alınması və statistik mübadilə tutumunun öyrənilməsi. Kimyanın aktual problemləri" // Ümummilli Lider Heydər Əliyevin anadan olmasının 96-ci ildönümünə həsr olunmuş XIII Beynəlxalq Elmi Konfrans, Bakı: -15-16 May, –2019. –s. 91-92.

15. Balayeva, O.O. Synthesis of zinc-aluminum mixed oxide/polyvinyl alcohol (ZnAl mixed oxide/PVA) and application in Pb(II) removal from aqueous solution / O.O.Balayeva, Azizov A.A., Muradov M.B. [et al.] // Journal of Dispersion Science and Technology. 2020. **Web of Science**.

16. Muradov, M.B., Formation mechanism of CdxZn1–xS / PVA nanocomposites by SILAR method / M.B.Muradov, L.R.Gahramanli, O.O.Balayeva, // Results in Physics, – 2020.18, – p. 1–9 **Web of Science.**

17. Balayeva, O.O., Azizov, A.A., Muradov, M.B., Alosmanov, R.M.. Synthesis and characterization of ZnAl-LDHs using different

base solutions // International Conference dedicated to 100th Anniversary of Azerbaijan State Oil and Industry University, -Baku: -24-25 December, –2020. –p. 98-100.

18. Balayeva, O.O. Sink oksid və qarişiq oksid (ZnO və $Zn_6Al_2O_9$) / PVS nanokompozitinin Pb^{2+} ionlarının sorbsiyasina tətbiqi / O.O.Balayeva, A.Ə.Əzizov, M.B.Muradov [və b.] // Bakı Universitetinin Xəbərləri. Təbiət elmləri seriyası, Azərbaycan – 2021.1, – p. 25-32.

19. Abdullayeva, G.X., Azizov, A..A., Balayeva, O.O., Buniyatzade, I.A. [et al.] Adsorbsion and photodegradation of orange g dye by CoAl LDH /PVA and copper doped coal ldh/pva nanocomposites under visible light // 7th International Conference MTP – 2021: Modern Trends in Physics, -Baku: -15-17 December, – 2021. 2, –p. 119-121.

20. Paşayev N.V., Əzizov, A.Ə., Balayeva, O.O., R.M.Alosmanov. BNK/seolit funksional kompiziti ilə metal ionlarının məhluldan sorbsiyasinin öyrənilməsi // V international scientific conference of young researchers Baku Engineering University, -Baku: -29-30 April, – 2021. –p. 1036-1038.

21. Balayeva, O.O., Əzizov, A.Ə., Alosmanov, R.M., Bünyatzadə İ.A. CoAl-layli ikili hidroksidlər pvs nanokompozitinin sintezi // V International Scientific Conference of Young Researchers. Baku Engineering University, -Baku: -29-30 April, – 2021. –p. 1039-1040.

22. Balayeva, O.O., Azizov, A.A., Muradov, M.B., Alosmanov, R.M. Synthesis of ZnAl-layered double hydroxide by different reaction parameters // VIII International Scientific Conference «The Chemistry of Coordination Compounds» dedicated to the 85th anniversary of the Department of Analytical Chemist, -Baku: -22-23 December, – 2021. –p. 293-295.

23. Balayeva, O.O., Azizov A.A., Muradov M.B., Alosmanov R.M. Removal of tartrazine from aqueous solution by ZnAl-LDH/PVA nanocomposite // 1st international congress on natural sciences (ICNAS-2021)”, -Erzurum: -10-12 September, – 2021. –p. 176.

24. Paşayev, N.V., Əzizov, A.Ə.. Balayeva, O.O. Butadien nitril kauçukunun seolitlə funksional kompozitinin yuyulmasi və alinan

maddənin iştiraki ilə metal ionlarinin sorbsiyasinin öyrənilməsi // Ümummilli Lider HEYDƏR ƏLİYEVİN anadan olmasının 98-ci ildönümünə həsr olunmuş XIV Beynəlxalq Elmi Konfransı, -Bakı: -25-26 May, – 2021. –s. 96-97.

25. Алиев, О.И., Балаева, О.О., Азизов, А.А. Исследование адсорбции тартразина на нанокомпозите ZnAl-СДГ/ ПВС // Ümummilli Lider Heydər Əliyevin anadan olmasının 98-ci ildönümünə həsr olunmuş gənc tədqiqatçıların «Kimyanin Aktual Problemləri» XIV Beynəlxalq Elmi Konfransı, -Bakı: -25-26 May, – 2021, –s. 97-98.

26. Abdullayeva G.X., Balayeva, O.O., Əzizov A.Ə. CoAl əsaslı laylı ikili hidroksidlərin kationit və anionit xassələrinin öyrənilməsi // Ümummilli Lider Heydər Əliyevin anadan olmasının 98-ci ildönümünə həsr olunmuş gənc tədqiqatçıların «Kimyanin Aktual Problemləri» XIV Beynəlxalq Elmi Konfransı, -Bakı: -25-26 May – 2021. –s. 109-110.

27. Abdullayeva, G.X., Əzizov, A.Ə., Balayeva, O.O. CoAl-layli ikili hidroksidlər PVS nanokompozitinin sintezi // V International Scientific Conference of Young Researchers. Baku Engineering University, -Baku: -29-30 April, – 2021. –s. 1039-1040.

28. Məmmədova, S.F., Balayeva, O.O., Əzizov, A.Ə., Muradov, M.B. $Ni_{0.2}Zn_{0.8}S$ nanohissəciklərinin layli ikili hidroksidlər əsasinda alinması // Ümummilli Lider Heydər Əliyevin anadan olmasının 98-ci ildönümünə həsr olunmuş doktorant, magistrant və gənc tədqiqatçıların «Kimyanin Aktual Problemlərİ»XIV Beynəlxalq Elmi Konfransı, Bakı: -25-26 May, – 2021. –s. 86-88.

29. İmaməliyeva, N.N., Balayeva, O.O., Əzizov A.Ə., Muradov M.B. Mis kadmium sulfid ($CuCdS_2$) nanohissəciklərinin funksionallaşdirilmiş nitril kauçuku əsasinda alinmasi // Ümummilli Lider Heydər Əliyevin anadan olmasının 98-ci ildönümünə həsr olunmuş doktorant, magistrant və gənc tədqiqatçıların «Kimyanin Aktual Problemləri» XIV Beynəlxalq Elmi Konfransı, -Bakı, -25-26 May – 2021. –s. 91-93.

30. Balayeva, O.O., Əzizov, A.Ə., Muradov, M.B., Mammadova, S.F. Controllable synthesis of $Ni_xZn_{1-x}S$ nanoparticles on the base of NiZnAl Layered Double Hydroxide/PVA composite matrix // 2nd

International Conference on Light and Light-based Technologies (ICLLT), -Ankara: -26– 28 May –2021. –p. 119.

31. Balayeva, O.O. Adsorption and photodegradation of quinoline Yellow, ponceau 4R and brilliant blue FCF onto ZnAl LDH – LDO / PVA nanocomposite // Georgian Technical University 6th International Conference “Nanotechnology”GTU nano 2021 In memory of Prof. Alex Gerasimov, -Tbilisi: - 4-7 October – 2021. –p.11-12.

32. Balayeva, O.O., Azizov, A.A. ZnAl-LDH/PVA nanocomposite for efficient photocatalytic degradation of ponceau 4r // 1st International symposium on recent advances in fundamental and applied sciences. Atatürk University Faculty of Science, -Erzurum: -10-12 September, –2021. –p. 182.

33. Balayeva, O.O. Synthesis and characterization of zinc-aluminum based layered double hydroxide and oxide nanomaterials by performing different experimental parameters. Journal of Dispersion Science and Technology, United States –2022. 43(8), –p.1187-1196. **Web of Science**.

34. Balayeva, O.O. Removal of tartrazine, ponceau 4R and patent blue V hazardous food dyes from aqueous solutions with ZnAl-LDH/PVA nanocomposite / O.O.Balayeva, A.A. Azizov, M.B. Muradov. // Journal of Dispersion Science and Technology, –2022. 1, –p. 1-14. **Web of Science.**

35. Balayeva, O.O. Photocatalytic degradation of Ponceau 4R by ZnAl-layered double hydroxide nanostructures obtained with and without polyvinyl alcohol. Journal of the Chinese Chemical Society, –2022. 1, –p. 1594-1607. **Web of Science.**

36. Gahramanli, L. Structural, Optical, and Electric Properties of $Cd_xZn_{1-x}S$ Nanomaterials by Sonochemical and Sılar Methods / L.Gahra-manli, O.O. Balayeva, M.Muradov//Journal of Inorganic and Organo-metallic Polymers and Materials, –2022.–p. 3395–3406.**Web of Science.**

37. Gahramanli, L.The impact of electrolyte solution concentrations on the optical characteristics of CdS nanoparticles / M. Muradov, O.O.Balayeva [et al.] // International Journal of Modern Physics B, Singapore –2022, –p. 2350103. **Scopus.**

38. Balayeva, O.O. Synthesis, properties and practical applications of doped and undoped, zinc-containing layered double hydroxides–A Brief Review. NNC RK Bulletin, Kazakhstan–2022. 3, –p. 45-55 **CrossRef.**

39. Balayeva, O.O. Sink-alüminium layli ikili hidroksidlərin polivinil spirti ilə nanokompozitlərinin hazırlanması Bakı Universitetinin Xəbərləri. Təbiət elmləri seriyası, Azərbaycan –2022. 3, –p. 26-33.

40. Balayeva, O.O. Synthesis of different metal doped ZnAl-LDH/PVA nanocomposites for adsorption and photocatalytic application. NNC RK Bulletin, Kazakhstan –2022. 4, –p. 63-73 **CrossRef.**

41. Balayeva, O.O. Kobalt alüminium layli ikili hidroksid / polivinil spirti nanokompoziti ilə Narinc G boyaq maddəsinin sulu məhlullardan adsorbsiyasi və fotokatalitik parçalanması / G.X.Abdullayeva, A.Ə.Əzizov, O.O.Balayeva // Bakı Universitetinin Xəbərləri. Təbiət elmləri seriyası, –2022. №4, –s. 5-11.

42. Balayeva, O.O., Azizov, A.A., Muradov, M.B., Alosmanov, R.M. ZnAl-LDH nanocomposite obtained with and without PVA // International Health, Engineering and Sciences Congress. Ankara, 7-8 May - 2022. –p. 161-162.

43. Balayeva, O.O. Synthesis and photocatalytic performance of ZnAl-LDH/PVA Nanocomposite // Mediterranean International Conference on Research in Applied Sciences, -Antalya: - 22-24 April, –2022. –p. 482.

44. Mustafayeva, N., Balayeva, O.O., Əzizov A.Ə., Alosmanov R.M. Modifikasiya olunmuş ZnAl əsasli layli ikili hidroksidlər üzərində ponso 4r boyaq maddəsinin sulu məhlullardan fotokatalitik parçalanmasi // Ümummilli Lider Heydər Əliyevin anadan olmasının 98-ci, gənc tədqiqatçıların «Kimyanin Aktual Problemləri» XIV Beynəlxalq Elmi Konfransı, -Bakı: -18-19 May, – 2022.418.

45. Yəhyayeva, Q.Y. Balayeva, O.O. CdZnAl LİH polimer kompozitinin fotokatalitik xüsusiyyətlərinin öyrənilməsi // Ümummilli Lider Heydər Əliyevin anadan olmasının 98-ci ildönümünə həsr olunmuş gənc tədqiqatçıların «Kimyanin Aktual

Problemləri» XIV Beynəlxalq Elmi Konfransı, - Bakı: -18-19 May, – 2022. –p. 419.

46. Abdullayeva, G.X., Əzizov, A.Ə., Balayeva, O.O., Buniatzadə, İ.A. CoAl LİH-lərin PVS-də nanokompoziti ilə narinc g boyaq maddəsinin sulu məhlullardan sorbsiyasi və fotokatalitik deqradasiyasi // Ümummilli Lider Heydər Əliyevin anadan olmasının 98-ci ildönümünə həsr olunmuş gənc tədqiqatçıların «Kimyanin Aktual Problemləri» XIV Beynəlxalq Elmi Konfransı, Bakı: -18-19 May – 2022. –p. 441-442.

47. İmaməliyeva, N.N., Balayeva, O.O., Əzizov, A.Ə., Alosmanov, R.M. FNK əsasinda sintez olunmuş mis kadmium sulfid nanohissəciklərinin fotokatalitik aktivliyinin öyrənilməsi // Ümummilli Lider Heydər Əliyevin anadan olmasının 98-ci ildönümünə həsr olunmuş gənc tədqiqatçıların «Kimyanin Aktual Problemləri» XIV Beynəlxalq Elmi Konfransı, Bakı: -18-19 May, – 2022.-p. 445.

48. Balayeva, O.O., Azizov, A.A., Muradov, M. B., Alosmanov, R.M. ZnAl-ldh nanocomposite obtained with and without PVA // I International Health, Engineering And Sciences Congress, -Ankara:, -7-8 May – 2022. –p. 161-162.

49. Balayeva, O.O., A. A.Azizov, M. B.Muradov, R. M.Alosmanov [et al.], Adsorption of patent blue v food dye by ZnAl-LDH/PVA nanocomposite // II International Health, Engineering and Sciences Conference, - Kayseri: -19-21 August, – 2022. –p. 108-109.

50. Balayeva, O.O., N.N. İmamaliyeva, A.A. Azizov, M.B. Muradov [et al.] Synthesize of copper cadmium sulphide ($CuCdS_2$) nanoparticles on the basis of functionalized nitrile butadiene rubber by SILAR method // 7 th International Conference MTP–2021: Modern Trends in Physics. -Baku: -15-17 December, – 2021. –p. 84-85.

51. Balayeva, O.O., N.N. Imamaliyeva, A.A. AzizovM. B. Muradov [et al.], SILAR Synthesis of $CuCdS_2$ Nanostructures for Photocatalytic Applications // 9th International Conference on Materials Science and Nanotechnology for Next Generation Gazi University, -Ankara: -22 - 24 September, – 2022. –p. 123.

52. Balayeva, O.O., Azizov, A.A., Muradov, M. B., Alosmanov, R. M. [et al.], Synthesis of ZnAl-layered double hydroxide / polyvinyl alcohol for photocatalytic degradation of ponceau 4R // International Conference: Modern Problems of Theoretical &Experimental Chemistry, Baku: - 29 - 30 September,– 2022. –p. 269.

53. Yahyayeva, G.Y., Balayeva, O.O., Hashimova S.C.. Investigation of adsorption and photodegradation properties of CdZnAl LDH / polymer nanocomposite // IV International Health , Engineering and Sciences Congress. Eskisehir, Turkiye 17-19 December – 2022. –p. 94.

54. Yahyayeva, G.Y., Balayeva, O.O. The investigation of the photodegradation of m-cresol on CdZnS and CdZnAl LDH / polymer nanocomposite // V International Health, Engineering and Sciences Congress, -Ankara: -19-21 March, –2022. –p. 207.

55. Balayeva, O.O. Synthesis of znal-ldh/pva nanocomposite and adsorption of patent blue v food dye from water solution / O.O.Balayeva A.A.Azizov, M.B.Muradov [et al.] // Azerbaijan Chemical Journal № 1 –2023. –p. 64–74 **Scopus**

56. Balayeva, O.O., Noncovalent doping of fullerene (C_{60}) into ZnAl–LDH/PVA matrix and photocatalytic degradation of methylene blue and congo red from water / O.O.Balayeva, A.A.Azizov, M.B .Muradov [et al.] // Journal of Inorganic and Organometallic Polymers and Materials, 2023, p.1-20. **Web of Science**.

57. Balayeva, O.O. Fullerene (C_{60})-doped zinc-aluminium layered double hydroxide/polyvinyl alcohol nanocomposites: Synthesis, characterization, and photodegradation of methylene blue from water solution / O.O.Balayeva, A.A.Azizov, T. Sh Israfilli // Journal of the Chinese Chemical Society. 2023. 1-14. **Web of Science.**

58. Balayeva, O.O. Preparation of fullerene – modified zinc – containing layered double hydroxide – polymer nanocomposites for photocatalytic applications / O.O.Balayeva, T.Sh.Israfilli // Ümummilli Lider Heydər Əliyevin anadan olmasının 100-cü ildönümünə həsr olunmuş gənc tədqiqatçıların « Kimya və kimya

Texnologiyası» II Respublika Elmi Konfransı, –Bakı: -04,05 may, –2023.

59. Yahyayeva Q.Y. CdZnS və CdZnAl-LİH/polimer nanokompo-zitinin sintezi və fotokatalitik aktivliyinin öyrənilməsi / Q.Y.Yahyayeva, O.O.Balayeva // Ümummilli Lider Heydər Əliyevin anadan olmasının 100-cü ildönümünə həsr olunmuş doktorant, magistrant və gənc tədqiqatçıların «Kimya və kimya texnologiyası» II Respublika Elmi Konfransı, –Bakı: -04,05 may, –2023.

60. Haşımova, S.C., Balayeva, O.O. Əzizov, A.Ə., Zn-Al layli ikili hidroksid əsasli kompozitlərdə metilen göyü, rodamin 6g, kristal bənövşəyi, brilyant yaşili boyaq maddələrinin sorbsiyasinin tədqiqi / Ümummilli Lider Heydər Əliyevin anadan olmasının 100-cü ildönümünə həsr olunmuş gənc tədqiqatçıların « Kimya və kimya texnologiyası » II Respublika Elmi Konfransı, –Bakı: -04,05 may, –2023.

61. Yahyayeva, Q.Y. Balayeva, O.O. CdZnS və CdZnAl-LİH/PVS nanokompozitinin sintezi və metilen göyü boyaq maddəsinin fotokatalitik parçalanmasının öyrənilməsi /Ümummilli Lider Heydər Əliyevin anadan olmasının 100-cü ildönümünə həsr olunmuş «Kimya və kimya texnologiyası » II Respublika Elmi Konfransı, –Bakı: -04,05 may, –2023.

62. Balayeva, O.O. Synthesis, structural and optical characterization of $Cd_xZn_{1-x}S$/FNBR nanocomposites / O.O.Balayeva, A.A. Azizov, M.B. Muradov [et al.] // Chemistry Select. 2024, p.1-17. **Web of Science.**

63. Balayeva, O.O. Synthesis and characterization of $Cu_xCd_{1-x}S$ nanocrystals into functionalized nitrile butadiene rubber matrix / O.O.Balayeva, A.A. Azizov, M.B. Muradov, [et al.] // Journal of the Chinese Chemical Society. 2024, p.1-15. **Web of Science.**

ABBREVIATIONS

ACTB - Ammonium citrate tribasic
BET - Brunauer-Emmett-Teller
NBR - Nitrile butadiene rubber
E_g - bandgap
EPR - Electron paramagnetic resonance

PL - Photoluminescence
FNBR – Functionalized (chlorophosphorilated) nitrile butadiene rubber
ICP-OES - Inductively coupled plasma - optical emission spectrometry
IR - Infrared spectroscopy
IPA - Isopropyl alcohol
XRD – X-ray diffractometer
JCPDS – Standard for XRD
CR - Congo red
LDH- Layered double hydroxide
MB – Methylene blue
NaSt - Sodium stearate
O2$^{\cdot -}$ - Superoxide anion
PB-V - Patent blue V
PVA - Poly vinyl alcohol
R6G - Rhodamine 6G
SD% - Sorption degree
PD%- Photodegradation degree
SEM - Scanning Electron Microscope
SILAR - Sequential adsorption and reaction of the ionic layer
ST - Sorption capacity
SA - Stearic acid
UV - Ultraviolet spectroscopy
UDM - uniform deformation model,
D-R – Dubinin-Radushkevich

The defense will be held on "21" June 2024 at 11:00 am at the meeting of the Dissertation council BED 2.16 of Supreme Attestation Commission under the President of the Republic of Azerbaijan operating at Baku State University.

Address: Republic of Azerbaijan, AZ 1148, Baku city, acad. Z. Khalilov street 23, Main building.

Dissertation is accessible at the Scientific library of Baku State University.

Electronic version of dissertation and its abstract are available on the official website of Baku State University (bsu.edu.az).

Abstract was sent to the required addresses on "20" May 2024

Signed for print: 14.05.2024
Paper format: A5 (60×90 1/16)
Volume: 76012
Number of hard copies: 30